Genetically Modified Collagen-like Triple helix Protein as Biomimetic Template to Fabricate Metal/Semiconductor Nanowires

by

Hanying Bai

A dissertation submitted to the Graduate Faculty in Chemistry in partial fulfillment of the requirements for the degree of Doctor of Philosophy, The City University of New York

2011

This manuscript has been read and accepted for the Graduate Faculty in Chemistry in Satisfaction of the dissertation requirement for the degree of Doctor of Philosophy.

Prof.Hiroshi Matsui, Hunter College_____
[require signature]

_____ _____
Date Chair of Examining Committee

Prof.Mahesh K. Lakshman__ _____
[require signature]

_____ _____
Date Executive Officer

Prof. Charles M. Drain, Hunter College_____

Prof. Ronald Koder, City College_____

Prof. Laura Kaufman, Columbia University____

Supervisory Committee

THE CITY UNIVERSITY OF NEW YORK

Abstract

Genetically Modified Collagen-like Triple helix Protein as Biomimetic Template to Fabricate Metal/Semiconductor Nanowires

By

Hanying Bai

Adviser: Prof. Hiroshi Matsui

Various metal and semiconductor nanowires have been developed as building blocks for electronics, optics, and sensors devices. Among these, new nanowires developed on biomolecular templates got more attention since the molecular recognition functions of these biomolecules with specific ligands can be employed to immobilize nanowires onto specific locations to establish desired device geometries. In order for their application in electronics, optics, and sensors device fabrications, after configuring device geometries with nanowires by the biomolecular recognition, we focused upon the biomineralization function of peptides on the nanotemplate sidewall to develop various material coatings such as metals and semiconductors for electronics and sensor applications. It should be noted that the coating morphology such as particle-domain size and inter-particle distance on the nanotemplates could be tuned by peptide sequences and conformations.

We launched the genetically modified recombinant collagen-like triple helix proteins as a biorecognition, size-controlling and rigid biotemplate. This collagen-like triple helix is the genetically engineered polypeptide assembly that contains a fragment from the

natural collagen sequence and has attractive features in hybrid nanomaterials. The length of the protein nanowire is uniform since it is determined by the number of amino acids. The length can be flexible if we genetically modify the sequence, which can also add chemical functionality by the genetic engineering procedure. Genetic engineering is more advantageous than the chemical synthesis for the functionalization /deritivization of peptide nanowire because only the desired specific residue of the peptide is functionalized by the genetic approach. The specific sequence can also increase stability so that the mechanical property can be tuned to be suitable for device application in harsh environment. By using the recombinant technology, it is possible to design and amplify a collagen-like triple helix that is monodisperse, easily mineralized with metal/ semiconductor precursors, and therefore can be applied as a rigid biomolecular template for metal/semiconductor nanowire fabrications. Moreover the production of triple helix can be large scaled up by means of the cell multiplication.

As continued work based on previous study of the application of C7 glycylglycine bolaamphiphilic peptide, the self-assembly of doughnut-shaped nanoreactors from monomer peptides with silica precursors was studied, and uniform size silica (SiO_2) nanoparticles were obtained. Possible mechanism in terms of chelating and catalysis functions of the peptide was formulated.

Keyword:

Collagen-like Triple Helix, Nanowire, Fabrication, Recombinant, Biotemplate.

This is

dedicated to

My wife: Wei Cai

谨以此文现予

我的爱妻： 蔡玮，和我的家人

Acknowledgements

First and above all, I'd like to give my wholehearted gratitude to my dear mentor, Prof. Hiroshi Matsui, for his inspiring guidance, unconditional devotion, and enlightening instructions in the joyful but challenging journey of my PhD study.

I also own thanks to my research committee members, Prof. Michael C. Drain, Prof. Laura Kaufmann and Prof. Ronald L. Koder. This dissertation cannot be so fruitful without their continuous guidance and advice.

As a research collaborator, I own special thanks to Prof. Yujia Xu and Dr. Ke Xu. Our collaborating has been enjoyable and fruitful.

I own thanks to my previous colleagues in our lab: Dr.Xueyun Gao, Dr.Roberto de la Rica, Dr.Nurxat Nuraje, Dr.Linglu Yang, Dr.Lingtao Yu, Dr.Robert Maccuspie, Dr.Anita Swami, Dr.Sangyup Lee, Dr.Anne Runge, Ms.Zheyuan Zhao, Ms.Fen Xu and current colleagues: Dr.Yoshiyaki Maeda, Dr.Jungsun Lim, Ms.Parminder Jeet Kaur, Mr.Cristophe Pejoux, Mr.Wei Su, Ms.Luona Anjia, Ms.Prerna Kaur, Ms.Menglu Shi, and Mr.Zengyan Wei. Especially I thanks for Dr. Roberto de la Rica kindly helping me to revise my dissertation. I own thanks to friends from other labs: Dr. Jorge Marolas, Dr. Areti Tsiola, Dr. Joshua Cheng, Dr.Dongguang Wei, Mr.Jia Ma and Mr.Andrew Mutter. Most of all, I own thanks to my dear parents: my mother: Ms. Shulan Kang and my father: Hongwen Bai, and my aunt: Ms. Jingwen Bai.

Finally, I want to express my gratitude to my wife, Wei Cai.

I also gratefully acknowledge the financial supports from DOE and NIH.

Thanks everybody

Hanying Bai

Table of Contents

List of Figures

List of Schemes

List of Tables

Chapter 1. Introduction to Genetically Modified Collagen-like Triple Helix Peptide

Recently, various metal and semiconductor nanowires have been developed as building blocks for electronics, optics, and sensors devices. Among these, newly developed nanowires grown on biomolecular templates got more attention since the molecular recognition functions of these biomolecules with specific ligands can be employed to immobilize nanowires onto specific locations to establish desired device geometries[6-8]. Most of the biomolecular-nanowire templates made from DNAs or peptides do not possess suitable electric properties for those devices, and therefore there is an extensive effort in the field of bionanotechnology to coat these addressable biomolecular nanowires with metals and semiconductors[9-16]. While these biomolecular-nanowire templates appear to be promising building blocks for nanodevices, it is essential to have size monodispersity, strength, and mass production to impact real-world applications. For example, biomolecular templates self-assembled from peptidic monomers tend to yield polydisperse materials with heterogeneous diameters and uncontrolled length through the self-assembly process. Double-stranded DNA[17], F-actin filaments0[18], peptide microtubules [19], amyloid fibres[20] and lipid tubules [21] as well as biological organisms (bacteria[22], viruses[23, 24], fungal colonies[25], etc.) have been employed as templates to fabricate structural functional inorganic materials, however certain problems appeared in terms of controlling certain parameters such as rigidity and large-scale-production seemed hard to ovecome[26]. For instance, the tobacco mosaic virus (TMV), a rod-shaped biomolecular template, had been applied for various metal coatings, but accurate control of the length with low dispersity is not an easy task[27-29]. Another

example, DNA biomolecular templates had defined lengths determined by the number of nucleic acids but lack conformational rigidity and have the tendency of supertwisting making it difficult to obtain rigid and straight nanowires[9]. Their production cost and time may also not be suitable for large-scale syntheses.

In this dissertation, we launch the genetically modified artificial collagen-like triple helix proteins as a biorecognition, size-controlling and rigid biotemplate and we discuss about its property and the fabrication nanowires for its applications in nanotechnology and materials.

The collagen has been studied for medical reasons. For example, the stability of triple helix, a building block for collagen fibrils, can be related to diseases such as osteogenesis imperfecta (OI) when the peptide sequence is modified by mutation [30]. However, this triple helix also has attractive feature in hybrid nanomaterials. The length of the peptide nanowire is uniform since it is determined by the number of amino acids. The length can be flexible if we genetically modify the sequence, which can also add chemical functionality via genetic engineering. The specific sequence can also increase stability so that the mechanical property can be tuned to be suitable for device application in harsh environments.

Introduction to Genetic Engineering and Recombinant Technology

The basic idea of genetic engineering is the technology of preparing recombinant DNA in vitro by cutting up DNA molecules, splicing together fragments and inserting this new genetic information into existing cells in order to modify a specific organism for the purpose of changing one of its characteristics or generating expected peptide/protein product via expression procedure[31]. Genetic engineering is more advantageous than

chemical synthesis for the functionalization/deritivization of peptide nanowires because a specific position of the peptide can be functionalized by this genetic approach whereas the chemical synthesis require blocking unwanted position to modify particular residue due to the lack of specificity of chemical reactions. This approach is becoming even more practical since genetic engineering has advanced to engineer proteins that incorporate non-natural amino acids. The capability of introducing these novel residues in a residue- specific or site-specific manner introduces the versatility for added functionality. The residue specific incorporation in which particular amino acids are replaced with non-natural peptide analogs induces the modification of the physical and the chemical properties of proteins. The incorporation of particular amino acid sequence into recombinant proteins emerges as an alternative strategy for the synthesis of artificial proteins that possess diverse chemical, physical and biological properties. Therefore, this expression system provides us with a perfect platform to investigate and insert any sequence based on its applicability.

Recombinant DNA technology in protein engineering is able to tether the functionalities of the protein[1, 31]. Figure 1.1 summarizes the process of protein synthesis via the recombinant technology[1]. After construction of the gene library, an individual gene is incorporated into a circular plasmid DNA vector, which can be used to transform an appropriate bacterial host. This circular plasmid DNA vector also contains an antibiotic resistant gene for the isolation of the gene of interest after the replication step. The selection of the specific type of vector depends on the copy number of plasmid, the size of the gene of interest to be ligated in the vector, and importantly the host system where the plasmid can replicate using the protein machinery system of the host. The

bacterial host *Escherichia coli* (*E. coli*) is the most commonly used because of the simplicity and the efficiency of *E.coli* to grow in a wide range of conditions[31, 32]. The plasmids are replicated during every division of bacterial cells. The plasmids of individual bacterial colonies can be screened primarily on the basis of the presence of the antibiotic resistant gene in the plasmid. To isolate the specific artificial genes, cells are cultured in the media containing antibiotics and the cells who survive should contain the plasmid of interest. This plasmid encodes the DNA sequence for the desired fusion protein. The selected artificial gene is first analyzed to verify its DNA sequence. This plasmid expresses and produces fusion proteins that contain a promoter site for the recognition by mRNA polymerase, which regulates the transcription of the gene. This expression plasmid is re-introduced into the bacterial host, and the host cells can be grown to achieve the high cell density. During this process, the plasmid switch is turned off in order to prevent the protein production from our gene of interest because premature production of proteins could be detrimental to the cell growth. After sufficient cell density is reached the switch is turned on (a process called induction) and the expression of the desired protein begins. Often the synthesis of other cellular proteins is slowed dramatically after induction.

Figure 1.1 Process of genetic engineering for protein design[1].

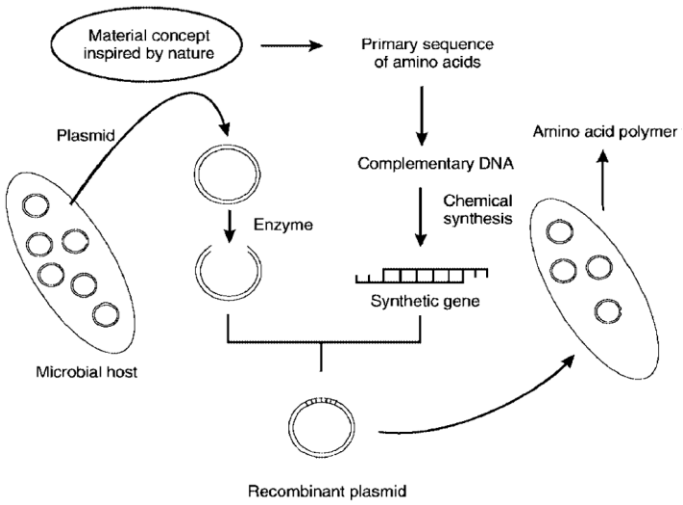

Introduction to Collagen and Triple Helix Stability

Collagen—Collagen is abundant in animal tissues in the long fibril form with a characteristic periodic structure in the axial direction [33-35]. The collagen fibrils provide the major biomechanical scaffold for cell attachment and anchorage of macromolecules, thus defining and maintaining the form of tissues [2, 36, 37]. The collagen fibril formation is basically a self-assembly process[38, 39]. While this process is intrinsic to the peptides, it is also sensitive to cell-mediated regulation, particularly in young or healing tissues[40-42]. Until now, over twenty-seven types of collagen composed of specific *d*-chains encoded by over 40 different genes have been identified [11, 36, 39]. The most important groups are the fibrillar collagen types I, II, III, IV and V, which largely contribute to maintaining the structural integrity of organs and tissues by forming supramolecular architectures. Type I is the most abundant collagen type with 90% of abundance of all types of collagen. It forms the largest and strongest fibrillar component that provides tensile strength to bones,

skin, tendons and ligaments[2, 43-45]. Type II collagen is unique to articular cartillage and fibrocartilage, the vitreous body of the eye, and certain other organs. [46] Type III collagen is similar to the structure of type I but less abundant[10,47]. Type IV is a major component of all membranes as a scaffold and type V is found in some veins and arteries. Other types of collagens are also incorporated into the extracellular matrix (ECM)[48]. Collagens are not only structural components providing the mechanical strength to tissues but also offer various specific functions through their interactions with other matrix components (proteoglycans, fibronectin, laminin), secreted soluble factors (interleukin 2, von Willebrand factor, pigment epithelium-derived factor), and cell surface receptors (integrins, discoidin domain receptors, glycoprotein IV)[10].

The fibril-forming collagen molecules consist of an uninterrupted triple helix of approximate 300 nm in length and 1.5 nm in diameter flanked by short extra helical telopeptides [49-52]. The assembly of collagen molecules into fibrils is an entropy driven process, similar to that occurring in other protein self-assembly systems, such as microtubules [35, 37, 38, 53, 54] . These processes are driven by the loss of solvent molecules from the surface of protein molecules and result in assemblies with a circular cross-section, which minimize the surface area volume ratio of the final assembly. Although the broad principles of collagen fibril self-assembly are generally accepted, less is known about the molecular mechanisms of the assembly process. Fibril-forming collagens are assembled from soluble procollagens,[2] and this assembly is triggered by specific enzymatic cleavage of terminal propeptides with the procollagen metalloproteinases (Figure 1.2(a)). Without these proteinases the assembly of collagen fibrils would not occur.

Our interest in triple helix peptide nanowires in our interest for material applications is based on the motif of the type I collagen. In the type I collagen, the triple helix molecule is a heterotrimer comprising of two identical α1 chains and one α2 chain. The α1 and α2 chains are very similar with over 95% identity on amino acid sequence. Each α-chain contains over 1000 amino acids and has a molecular weight of approximately 95,000. These molecules of type I collagen have a length of slightly less than 300nm and diameter of about 1.4nm (Figure 1.2(b))[2].

Figure 1.2 Hierarchical structural organization of collagen with amino acid sequence at nano scale up to the scale of collagen fibers in microns [2].

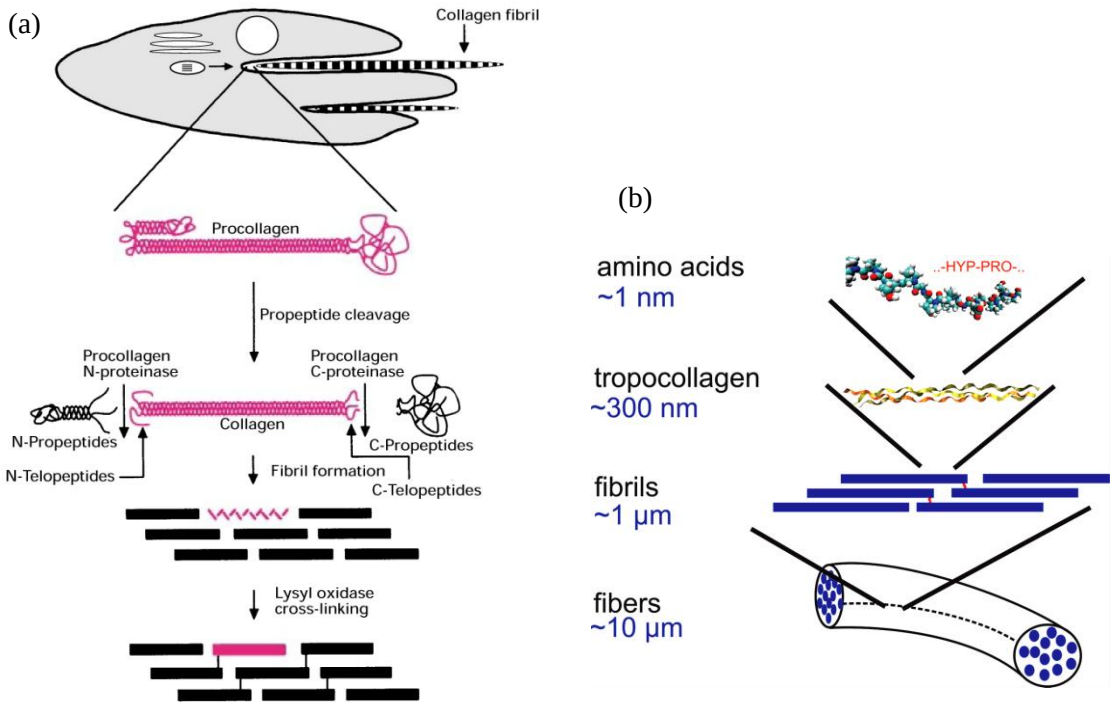

Conformation of Collagen — All types of collagen contain a unique tertiary structure of collagen triple helix and their conformation is important to assemble stable helical trimers for the application of rigid nanowire building blocks. The basic conformation consists of three polypeptide strands (called α peptides), each strand forms a left-handed polyproline II-like helix with all peptide bonds in *trans* conformation[33, 55]. These three left-handed helices, staggered by one residue relative to each other, are twisted together along a common axis into a right-handed cooperative coiled-coil structure, a triple helix, which is stabilized by numerous hydrogen bonds [10] . The triple helical regions of collagens are comprised of tandem repeats of Gly-Xaa-Yaa combination units. Isolated polyproline-II-helices are not stable if the polypeptide chains also contain other residues than proline (Pro) and hydroxyproline (Hyp)[44, 56-59] and therefore these hydrogen bonds have a major contribution to the stability of triple helix peptides. It should be noted that the right-handed α-helices left-handed polyproline-II-helices are relatively rare structural elements in proteins with the striking exception of collagens.[40] About one-third of X and Y positions are occupied with Pro and posttranslationally modified 4-hydroxyproline residues (Hyp), respectively. Such high content of imino acid residues enhances the thermal stability of the triple helix[48, 60].

Hydrogen bonding is a critical interaction for the triple-helix stabilization[61]. The triple helix has the hydrogen-bonding network on the repetitive backbone, but the repeating tripeptide unit consisting of three nonequivalent peptide groups differs from β-sheets or α-helices and all backbone peptide groups do not participate in the hydrogen-bonding[58]. All crystal structures show hydrogen bonds between the NH of Gly in one chain and the C═O of the residue at the X position of the neighboring chain[5, 62, 63]. When

the Y position is occupied by an amino acid rather than an imino acid, its amide group is hydrated by water molecules directed into the solvent, which reduces the contribution to stability[34, 38]. In addition, peptides with the sequence where the X position is occupied by a residue other than Pro, show second inter-chain hydrogen bonds between the amide group of the X position and the C═O of the Gly residue, which is mediated by one water molecule. It should be noted that the collagen triple helix has tightly bound water molecule around and this highly ordered hydration network contributes to maintaining the high density molecular packing in fibrils[60, 64]. This water network is biologically and physically significant with respect to molecular stability[33, 65-67].

Thermal Stability — Amino acid sequences can also be optimized to enhance the stability of triple helix peptides. Variations of the residues in the X and Y positions determine the global thermal stability and modulate the local stability and energy that are required for self-association, recognition, and binding [68, 69]. For example, the sequence of Gly-Pro-Hyp confers the maximal stability to the collagen triple helix. In general, the most stabilizing residues for the X position are Pro, Glu, Ala, Lys, Arg, Gln, and Asp, while the most stabilizing residues for the Y position are Hyp, Arg, Met, Ile, Gln, and Ala [41, 70-72]. The least stabilizing residues for both positions are the aromatic residues and Gly. The thermal stability of the 400 possible Gly-Xaa-Yaa sequences as compared to the Gly-Pro-Hyp sequence are presented in Table 1.1[2, 33]. In this table, there is a significant variation in thermal stability between the Gly-Pro-Hyp (T_m=47 ℃) and the Gly-Gly-Phe (T_m=20 ℃)[33, 73, 74]. This piece of result is an important asset in designing peptides that will form stable triple helices, as explained in the above paragraphs.

Table 1.1 Predicted (normal) and experimentally observed (bold) T_m values (℃) for all possible Gly-Xaa-Yaa combination units[2, 33].

X\Y	O	R	M	I	Q	A	V	E	T	C	K	H	S	D	G	L	N	Y	F	W
P	**47**	**47**	**43**	**42**	**41**	**41**	**40**	**40**	**40**	**38**	**37**	**36**	**35**	**34**	**33**	**32**	**30**	**30**	**28**	**26**
E	**43**	**40**	38	37	**38**	35	35	35	**36**	33	**35**	31	31	**30**	29	28	**30**	26	24	22
A	**42**	**38**	37	36	36	33	34	34	34	32	**31**	30	**33**	**33**	27	**28**	26	25	**22**	21
K	**42**	**39**	37	36	**39**	35	34	**35**	34	32	31	30	29	**36**	27	27	**32**	24	23	20
R	**41**	**41**	36	35	35	34	33	**34**	33	31	**30**	29	**31**	**35**	26	26	25	24	22	19
Q	**40**	**40**	36	35	34	34	33	33	33	31	**33**	29	28	27	26	26	25	23	22	19
D	**40**	**37**	35	34	34	32	33	33	33	31	**31**	29	28	27	26	26	25	23	21	19
L	**39**	39	34	33	**36**	31	32	31	31	29	**31**	27	27	26	25	27	23	22	20	18
V	**39**	39	34	33	33	33	32	31	31	29	**33**	27	27	26	25	24	23	22	20	18
M	**39**	39	34	33	33	32	31	31	31	29	**32**	27	26	25	24	24	23	22	20	17
I	**38**	38	34	33	32	34	31	31	31	29	28	27	26	25	24	24	23	21	20	17
N	**38**	38	34	33	32	32	31	31	31	29	28	27	26	25	24	24	23	21	19	17
S	**38**	38	33	32	32	32	31	30	30	28	28	26	26	25	24	23	22	21	19	17
H	**37**	36	32	31	31	30	29	29	29	27	26	25	24	23	22	22	21	19	18	15
T	**36**	36	32	30	30	30	29	29	29	27	26	25	24	23	22	22	21	19	17	15
C	**36**	36	31	30	30	30	29	29	29	27	26	25	24	23	22	22	21	19	17	15
Y	**34**	34	30	29	28	28	27	27	27	25	24	23	22	21	20	20	19	17	15	13
F	**34**	33	29	28	28	24	26	26	26	24	23	22	21	20	19	19	18	16	15	12
G	**33**	33	29	27	27	26	26	26	26	24	27	22	21	20	19	**25**	18	16	**20**	12
W	**32**	32	27	26	26	26	25	24	24	22	21	20	20	19	18	17	16	15	13	11

Quantification of the intrinsic propensities and interactions for the most common sequences can now be used as a basis for predicting stability of peptides and local stability in collagens. Comparison of the predicted stability of more than 20 peptides with observed T_m values shows there is good agreement in the majority of the cases [48].This is an important asset in designing peptides that will form stable triple helices, which are being used increasingly to map binding sites as well as for investigating interactions.

The stability of the triple helix peptide/protein for future biotemplates is especially important because wild type collagens are not stable enough to apply them as building blocks and could be damaged in extreme environments according to our previous studies[4]. Their mechanical property is also necessary to be enhanced to develop metal and

semiconductor coatings so that these triple helix peptide template nanowires can resist extreme chemical conditions.

Introduction to genetically-modified triple helix F877 peptide

Recently, we developed genetically-modified collagen-based triple helix peptides as templates for practical nanowires in various applications. In this peptide, the complete sequence of the recombinant collagen fragment F877 with the 63-residue region of the α1(I) (residue 877–939) is design to mimic the robust assembly of collagens[3, 5], as shown in Figure 1.3. To further increase the stability of the triple helix, repeating sequences of the tripeptide $(Gly\text{-}Pro\text{-}Pro)_n$ combination units with high triple helix propensity were added at both the C and N termini[5]. All together, the recombinant triple helix domain consists of 93 amino acid residues with the nanowire length of 40 nm.

A foldon and a Cys knot are the keys to nucleate the triple helix peptide. The C-terminal foldon domain from bacteriophage T4 fibritin works as the nucleation domain to facilitate the folding of the triple helix with two Cys residues (Gly-Pro-Cys-Cys-Gly) between the triple helix domain and the foldon domain[5, 75, 76]. When oxidized in the folded triple helix conformation, the Cys residues form a set of interchain disulfide bonds, also known as the Cys knot, further increasing the stability of the triple helix[5, 77]. The C-terminal part of the T4 fibritin trimer is formed from the trimeric coiled-coil domain, which is terminated by a C-terminal trimeric β-sheet propeller consisting of monomeric β-hairpin segments.[77] This β-propeller is necessary for the correct folding of the holoprotein and this foldon forms the β-propeller-like structure with a hydrophobic interior. The extensive hydrophobic interactions originate from the small β-sheets formed by three-fold-related β-hairpins[75, 76, 78]. In genetically-modified triple helix peptide, the C-

terminal foldon domain from bacteriophage T4 fibritin can be explored as the nucleation domain to facilitate the formation of the triple helix as an artificial trimerization domain[49, 75]. The C-terminal domain of T4 fibritin (foldon) is obligatory for the formation of the fibritin trimer structure. Simultaneously the three disulfide bonds are formed between the three chains by covalently oxidizing the cysteine residues into a disulfide knot. This method allows one to covalently link collagen-like peptides with the specific stereochemistry that occurs in Nature[68, 77]. Through this genetically modifying, this F877 collagen-like triple helix peptide was modified to become a rigid, rod-shaped molecule that is suitable for the application in building blocks of nano devices.

For the following the study in this dissertation on the artificial genetically modified triple helix we can presume that this tripe helix peptide from type I collagen can overcome many shortcomings of other biomolecular templates. The size of the entire triple helix protein molecule is very uniform and determined by the squence and can be modulated by genetic engineering. By using the recombinant technology, we can design and amplify a collagen-like triple helix that is monodisperse, easily mineralized with metal ions, and can, thus, be applied as rigid biomolecular templates for metal/ semiconductor nanowire fabrications in the critical reaction environment.

Figure 1.3 Illustration of the structure of F877 collagen-like triple helix protein. The amino acid sequence of the fragment F877 is shown in the upper panel. All the mutations are labeled on top of the sequence, and the two Gly→Ser substitution sites for fragments G901S and G913S are also underlined. The 14-residue Pro-free region is underlined, and the chymotrypsin digestion site Phe-935 is marked by the arrow. The residues introduced to form the Cys-knot are shown in italics. The gene expression construct of the fragments is shown in the bottom panel. The His-tagged thioredoxin was removed during the last purification procedure by thrombin digestion at the cleavage site APR marked by the triangle.[3, 5]

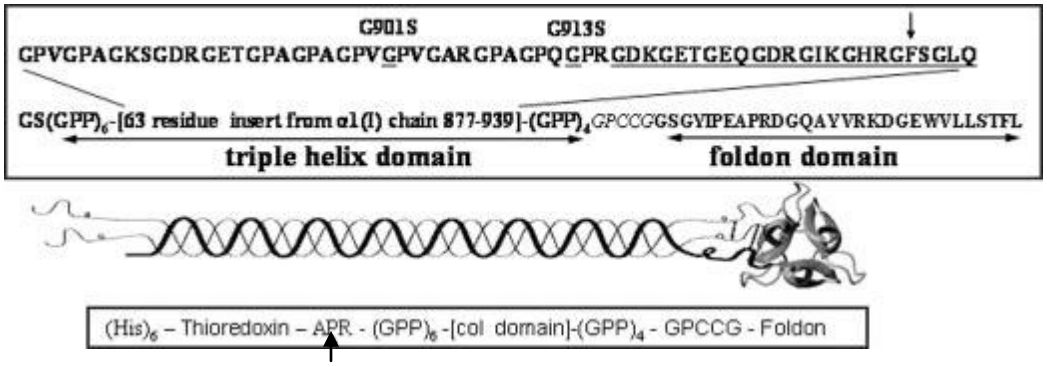

Chapter 2. Fabrication of Gold Nanowire in Uniform Length and Diameter Using Monodisperse and Rigid biomolecular Template, Collagen-like Triple Helix Proteins

Introduction

Recently, various metal and semiconductor nanowires have been developed as building blocks for electronics, optics, and sensors. Among these newly developed nanowires, nanowires grown on biomolecular templates such as DNA and peptide assemblies have shown an advantage since the molecular recognition functions of these biomolecules with specific ligands can be employed to immobilize nanowires onto specific locations in order to establish desired device geometries[8, 79, 80]. However, most of the biomolecular nanowire templates made from DNAs or peptides do not possess suitable electric properties for those devices, and therefore there is an extensive effort in the field of bionanotechnology to coat these addressable biomolecular nanowires with metals and semiconductors[81-93]. Recently, the morphology of the coating on these peptide nanotube templates could be controlled by means of specific peptide sequences and conformations so that the electronic structures of the resulting nanowires could be finely tuned for their device applications[94-96]. While these biomolecular nanowire templates appeared to be promising building blocks for nanodevices, it is essential to have size monodispersity, strength, and mass scale production in order to impact real-world applications. For example, biomolecular templates self-assembled from peptide monomers tend to yield polydisperse materials with heterogeneous diameters and uncontrolled length through the self-assembly process, however accurate control of length with low dispersity is not an easy task[97, 98]. Other biomolecular templates such as

DNAs, have defined lengths determined by the number of nucleic acids but they lack conformational rigidity. Furthermore, the production cost and time may also not be suitable for large-scale syntheses.

Fabricating hybrid nanomaterials by using bio-mimetic approach has tremendous impact not only in medicine and diagnostics but also in biomaterials science with growing interest in using the toolbox of genetic engineering in an exquisite manner[99]. The incorporation of non-natural amino acids into recombinant proteins emerges as an alternative strategy for the synthesis of artificial proteins that possess diverse chemical, physical and biological properties. By using recombinant technology to enhance the rigidity, the genetically modified collagen-like triple helix having uniform size was utilized as a template to make nanowires, which appeared to overcome the shortcomings of other biomolecular templates.

Here we report on a new application using collagen-like triple helix as a template to make gold nanowires. The collagen-like triple helix is the genetically-engineered polypeptide assembly that contains a fragment from the natural collagen sequence. Our study demonstrated that by using the recombinant technology, we can design and amplify collagen-like triple helix that is monodisperse, easily mineralized with metal ions and can, thus, be applied as rigid biomolecular templates for metal nanowire fabrications. Collagens are the major components of extracellular matrices for bones, cartilages, skins, blood vessels and corneas, and they are the most abundant proteins in higher organisms with superior mechanical properties[100-102]. The collagen-like triple helix is made of three polypeptide chains tightly twisted and bundled together to form a rigid, rod-shaped molecule, suitable for the applications in building blocks of nanodevices.

To explore the application of collagen-like triple helix as a nanowire template we studied the properties of three recombinant triple helix molecules obtained from an *E. coli* expression system (Figure 1.3). The three recombinant triple helices, F877,G901S and G913S, all contain a foldon domain taking from bacteriophage T4 fibritin, which serves as the nucleation site for the formation of the triple helix[103]. The triple helix domain of F877 consists of 63 amino acid residues modeling the region starting at the position 877 (from the N-terminus) of the α1 chain of type I collagen. To increase the thermal stability of the triple helix, repeating tripeptide (Gly-Pro-Pro) combination units sequences were added at the ends of the 63 residues. A pair of Cys residues was inserted at the interface of foldon and the triple helix domain in order to covalently link the three chains of the triple helix through a set of interchain disulfide bonds[102]. Triple helix G901S and G913S contain the same sequence as F877 except one Gly→Ser substitution at position G901S and G913S (G in Figure 1.3)[5, 62]. Replacing the obligatory Gly at every third position by any other amino acid residues with bulkier side chains is known to affect the triple helix conformation, and such mutations have been implicated in connective tissues diseases[5, 104]. There were circular dichroism spectral study for these three triple helix molecules as shown in Figure 2.2(a), the small positive peak at ~225 nm and the deep negative peak at ~197 nm are typical of the collagen triple helix [5]. The three recombinant molecules form a triple helix conformation in solution (Figure 2.2(b)) at 4 °C [3, 5].The triple helix behaved as a cross-linked trimer with no signs of further association based on the study using analytical ultracentrifugation and gel-filtration[9, 105]. The temperature of the thermal transition (T_m) of F877 is about 42 °C, significantly higher than that of native type I collagen (slightly lower than 37°C). The Gly → Ser substitution

at aa-901 decreases the thermal stability of F877 and reduces the T_m by ~10 ℃, while the overall unfolding profile remains similar.[9] In contrast, the Gly → Ser substitution at aa-913 in G913S affects both the value of T_m and the shape of the unfolding diagram. The melting curve reveals two steps in the unfolding prcocess. The first step occurs at a relatively lower temperature range, between 15 and 25 °C, and involves the decrease of about 40% of the ellipticity at 225 nm. The second melting step takes place between 29 and 35 °C causing the complete unfolding of the triple helix domain. Without the inclusion of the external structures other than triple helix, the backbone of triple helix would be much weaker and unfolding would occur at temperature lower than room temperature[5]. It can be concluded that the foldon, the Cys-knot and the repeating Gly-Pro-Pro structures significantly sustain the stability and rigidity of the entire triple helix protein and it is necessary to keep these three stabilizing structures in future artificial collagen-like triple helix protein.

The structure of the F877 triple helix was imaged by a transmission electron microscope (TEM) as shown in Figure 2.3(a). The triple helical F877 formed monodisperse, straight nanowires with an average length of 40 nm and no bending, indicating a rather rigid conformation. The length of the triple helix observed under TEM agrees well with the value of the ~ 35 nm end-to-end distance of a single triple helix consisting of 93 amino acids and a foldon domain estimated from the crystal structure of the triple helix[106]. The observed diameter of 4 nm appeared to be larger than the 1-2 nm predicted from the crystal structure. This slightly larger diameter in TEM image could be caused by swelling via hydration[107]. When comparing with TEM images, the triple helix G901S had the similar dimension as the F877 but appeared to disperse slightly more as

shown in Figure 2.3(b). The triple helix G913S had slightly longer size at ~50 nm compared with F877 and G901S due to its less stable structure and partial dissociation of triple helix structure starting from aa-913[5, 68].

Figure 2.1 SDS-PAGE(sodium dodecyl sulfate polyacrylamide gel electrophoresis) analysis of the expression of F877 fusion protein.

Lane 1: Extracted protein sample from non-transformed host cell (JM109)

Lane 2: Extracted protein sample from transformed and non-induced cell

Lane 3: Extracted protein sample from transformed and induced cell with 0.1mM IPTG

Lane 4 and 9: Protein molecular weight marker (66kD, 45kD, 36kD, 29kD, 24kD, 20kD, 14.2kD)

Lane 5: Purified protein by Co^{2+} – His affinity column

Lane 6: Purified protein from Lane 5 with thrombin cleavage

Lane 7: F877 protein with 20 mM DTT

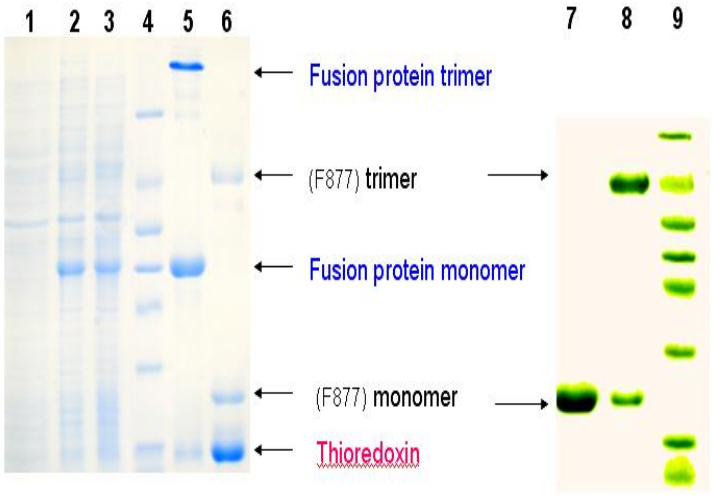

Figure 2.2 (a) CD spectra of collagen fragments of F877, G901S and G913S. The CD spectra of F877 (square), G901S (circle), and G913S (triangle) were taken at 4 ℃ with a concentration of 0.2 mg/ml; all data are normalized to molar ellipticity. (b) Temperature melt curves of the collagen fragments. The thermal unfolding of F877 (square), G901S (circle), and G913S (triangle) was monitored by the temperature-induced decrease of the CD signal at 225 nm, and normalized to the fraction folded of the triple helix protein.[3, 5]

(a)

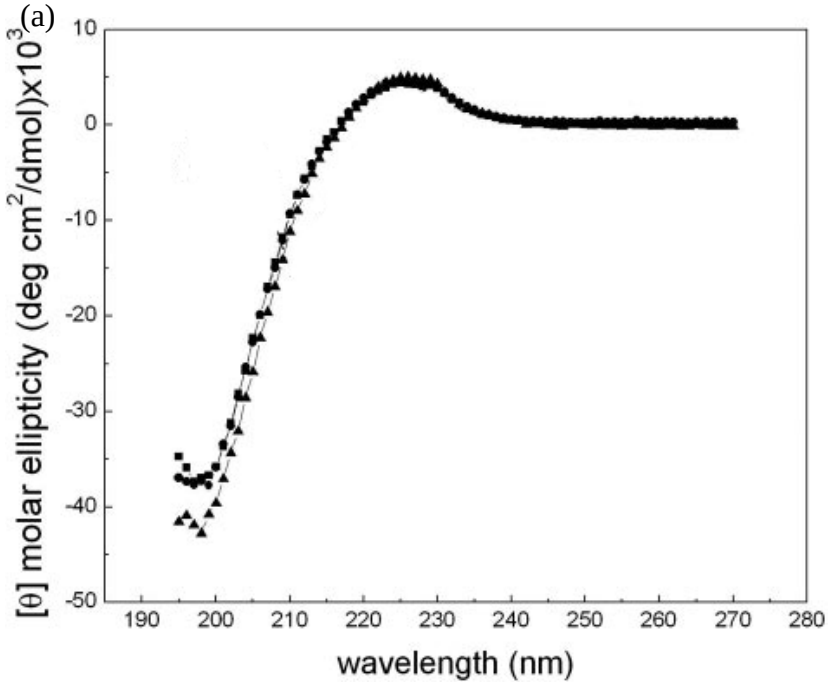

(b)

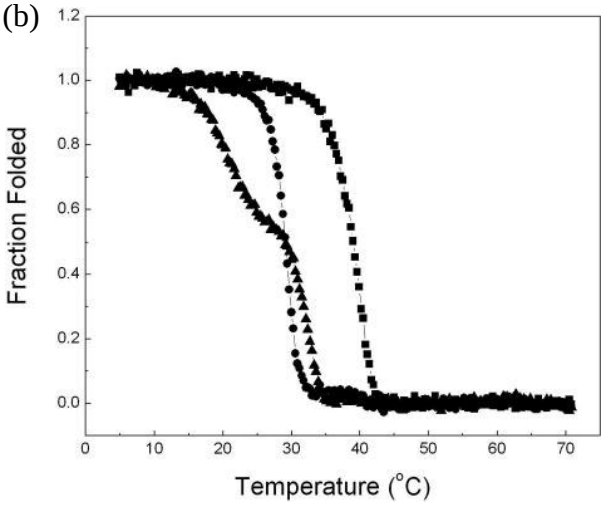

Figure 2.3 TEM image of (a) the F877 triple helix fragment; (b) the G901S triple helix fragment and (c) the G913S triple helix fragment. Scale bar = 40 nm.

(a) 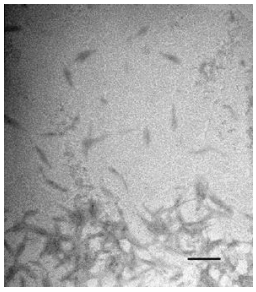 (b) 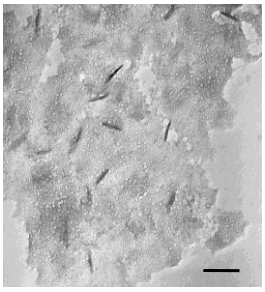 (c) 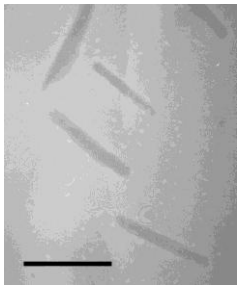

Experiments

Basic Procedure of Synthesis of Triple Helix Protein — The collagen fragments were cloned into a GPP-foldon vector built on the pET32a(+) plasmid of Novagen (the original GPP-foldon vector was kindly provided by Dr. Jurgen Engel at University of Basel, Switzerland). The product of this plasmid is a fusion protein with 6 x His tag and Trx tag (thioredoxin) as the carrier protein which can be removed by Thrombin cleavage to produce the final protein containing the triple helix domain and the foldon domain with the Cys-knot was inserted at the interface of the two domains. The protein was expressed in bacteria JM109 from Promega or bacteria BL21(DE3) from Novagen induced by IPTG (isopropyl β-D-1-thiogalactopyranoside) when concentration of bacteria reached certain level. Then the protein was purified by His-tag affinity column. After the His-tagged thioredoxin was separated with triple helix part by thrombin digestion, the fragments was further purified by HPLC to isolate the cross-linked triple helix. The final samples are >97% pure as estimated by SDS-PAGE (sodium dodecyl sulfate polyacrylamide gel electrophoresis) and gel-filtration experiments as shown in Figure 2.1.

Purification of F877/G901S/G913S Fusion Protein — We get 8 ml of nickel-affinity agar resin solution(Qiagen Co.), spin it down, remove the supernatant and wash the resin by 8~10 ml wash/extract buffer. We spin down, remove the supernatant and pour the lysate supernatant into the tube having resin. We seal this tube by parafilm, put it on the shake in the big freezer (3~4 ℃) and make the nickel resin bind with the His-tag of fusion protein for 1 hour. Then we centrifuge the tube under 4 ℃ at speed of 3000 rpm for 4 minutes. The supernatant (non-binding) is transferred to a new tube and the SDS sample for the supernatant is prepared. Meanwhile we add 10 ml of wash buffer (50 mM Tris, 300 mM NaCl and 20 mM imidazole pH 7) to the resin and transfer all to the separation column (15 ml or 20 ml volume). The column is fixed on a shaker and shaked for 10 min at 4 ℃. Then we fix the column on a stand, switch on the shutter and wash the resin by draining down all the liquid. 10~12 ml elution buffer (50 mM Tris ,300 mM NaCl and 250 mM imidazole pH 7) is utilized to wash the resin in the column and 8~9 eppendorf tubes are prepared to collect the eluate results. When elution buffer is present, resin color will become darker. Normally the 1^{st} ,2^{nd} and 3^{rd} tubes are blank and the 5^{th} or 6^{th} tube has the highest amount of fusion proteins. Because the resin can be reused, we use 15 ml of 0.5 M NaOH to the column to wash for 30 min[108]. The resin can be saved in the storage buffer (30% ethanol solution) [108].

Au Nanowire Fabrication — To grow Au nanocrystals on these three triple helices, first we mixed 200 μl of the triple helix solutions (0.2 mg/ml) with 535 μl of pH8.6 Tris buffer solutions (0.01 mol/l) and the mixtures were vortexed for 10 s and left 1 day at 4 °C. After 1.8 mg of trimethylphosphinegold chloride, $AuPMe_3Cl$, (Sigma) was incubated for 4 days at 4 °C, supernatant of the solution containing unattached Au salts was

removed by a pipette and then 5 μl of hydrazine hydrate (Sigma) was added to reduce Au salts on triple helices. To coat the HRE peptides (GenScript Corp., NJ) on triple helices, we mixed 200 μl of triple helix solutions with 535 μl of HRE solutions (3.9×10^{-4} mg /ml) in the pH8.6 or pH7.0 Tris buffer solutions for 1 day at 4 °C. After immobilization of HRE was confirmed by FTIR, we applied the same Au growth procedure described above to coat Au on the HRE-immobilized triple helices. After one day of the reduction at 4 °C, 3 μl of triple helix solutions were taken out to prepare TEM samples. Meanwhile the parallel batches of HRE-immobilized triple helix complex reacted with precursor for longer time as eight days and twenty-five days and for shorter time as two days and three days in order to study the kinetics of Au crystals. After incubation proceeded for these days, we separated the supernatant out of unreacted Au salt and added same amount of hydrazine to reduce the Au. After one reduction, TEM samples were prepared. The sample solutions were dried on carbon-coated copper TEM grids and excess solutions were removed by filter papers. These dried samples were then studied by transmission electron microscope (TEM) and electron diffraction (JOEL 1200 EX) at an acceleration voltage of 100 kV.

Figure 2.4 TEM images of the F877 triple helix peptides (a) in neat, (b) coated by Au, (c) coated by HRE-mineralizing peptides. (d) TEM image of the HRE-coated triple helix peptides (c) coated by Au. Electron diffraction patterns of (b) and (d) are shown next to their TEM images. Scale bar = 40 nm. Insets are their HRTEM images. Scale bar = 15 nm. [3]

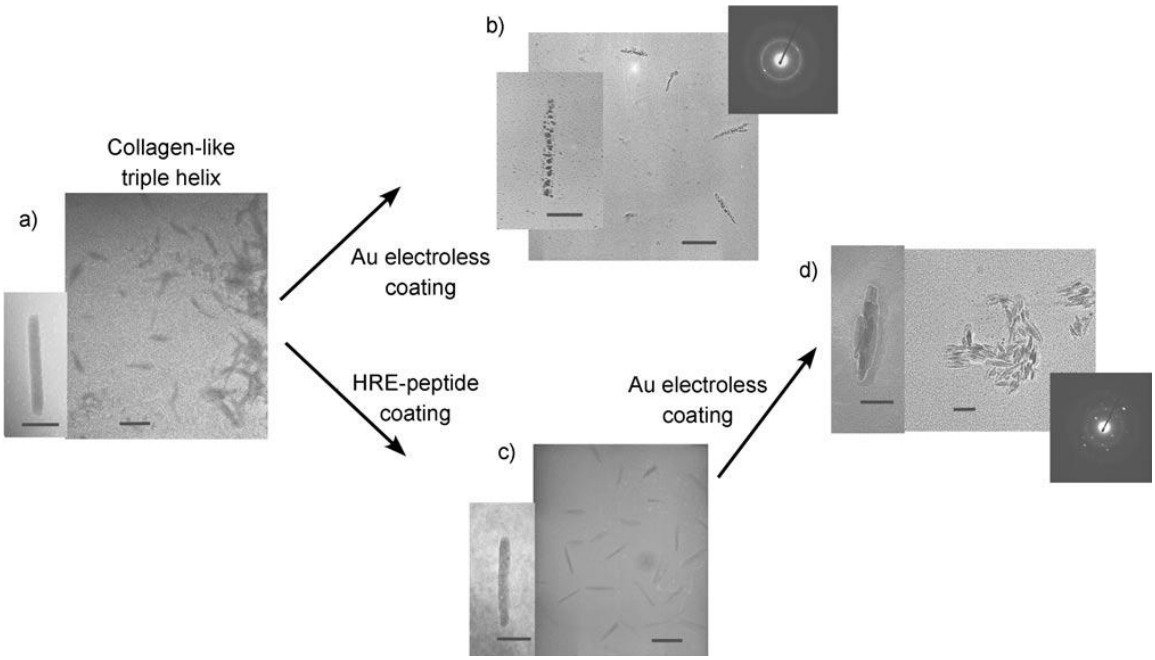

Results and Discussions

In order to examine feasibility in their application as building blocks for electronics, these triple helices were coated by Au. When the F877 triple helix (Figure 2.4(a)) was incubated with trimethylphosphinegold chloride ($AuPMe_3Cl$) and hydrazine hydrate for 4 days at 4 °C, Au crystals were grown on the helix as shown in Figure 2.4(b). This TEM image shows that the Au nanocrystal growth was localized on the helix surface. In order to grow Au on the triple helix more uniformly, we pre-coated the triple helix with Au-mineralizing peptide, Ala-His-His-Ala-His-His-Ala-Ala-Asp (HRE), which has a high affinity for organic Au salts[91, 109]. Our previous study demonstrated that the HRE bound glycine-bolaamphiphile nanotubes through hydrogen bonding at the amide groups of the nanotube after a simple incubation process[8]. The subsequent Au electroless process on these HRE-bound nanotubes yielded the uniform Au nanocrystal coating[91]. Similar enhanced, more uniformed mineralization was found with triple helix, F877, G901S and G913S, after incubation with HRE. When the F877 triple helix (Figure 2.4(a)) was incubated in the HRE peptide solution for 24 hrs, the triple helix was coated by the HRE peptide, confirmed by FTIR spectrometry[3]. No significant changes in length, diameter, and shape were detected after the triple helix was coated by HRE, as shown in Figure 2.4(c). The HRE peptide-coating increased dispersion of the triple helix protein molecules, presumably because the coating of HRE peptide containing cluster of positive charges reduces the potential attractive interaction between the triple helices. The reduction of Au on the HRE-coated triple helix produced uniform and highly crystalline Au coating on the surface, as shown in Figure 2.4(d). The Au-coated triple helix in the inset of Figure 2.4(d) appears to be a rice-like oval shape, which could be due to the

inhomogeneous coating of HRE peptide at the ends. As shown in Figure 1.3, the foldon at the C-terminal end forms a three stranded β-hairpin propeller, a conformation very different from that of the triple helix; the helix fray at the N-terminal end of the triple helix domain has been well documented by structural studies of crystallography and NMR[106]. These conformation differences likely resulted in different binding of the HRE peptides and leading to less Au growth on those areas as compared to the middle part of triple helix, consistent with the rice-shape formation. Similarly, Au nanowires with identical features were obtained when the G901S and G913S triple helix peptides were pre-coated by HRE, the only difference was that G901S yielded nanowires at pH 8.6 and G913S at pH 7.0. Moreover the yield of Au nanowires from G901S and G913S was less than from F877, which means that G901S and G913S were less rigid and less robust to resist the harsh reaction conditions and this result was consistent with the stability results shown before. Since G913S had less stability compared with F877 and G901S, pH 7.0 was the most suitable condition for G913S triple helix.

While the Au growth was observed with both the HRE pre-coated and the neat (i.e., no HRE pre-treatment) F877 triple helices, the reduction of Au with the neat G901S and G913S helix yielded no Au nanowires. The Gly→Ser mutation included in the G901S and G913S is known to cause the brittle bone disease due to the disruption of the triple helix conformation[104]. While the G901S and G913S were shown to adapt to the triple helix conformation at low temperature, the denaturation temperature (T_m) of these two triple helices was decreased (shown in Figure 2.2(b)) as compared to the F877, indicating the reduced stability of G901S and G913S with an altered conformation. It is unclear at this point whether the lack of Au deposit on the G901S or G913S is due to the disruption

of the charge distribution on the surface of the F877 triple helix or the altering of other structural features of the F877 triple helix caused by the Gly→Ser mutation. Nonetheless, the mutation caused variations of the Au crystal morphologies on the triple helix highlighted the dependence of the properties of the nanowires on the molecular conformations of the helix template. Such sequence dependent behavior also offers one a practical means to produce nanowires with desired properties by modifying the sequence of the recombinant triple helix molecules.

When Au precursor reacted with HRE-pre-coated F877 triple helix longer than four days, nanowires disappeared and bulky Au crystals were oberved. As inoculation time increased, Au crystals grew bigger; results of eight days' and twenty-five days' are shown in Figure 2.5(b) and (c). The oval shape nanowires become nucleation center of Au growth and more Au ion was trapped onto the surface which made the Au crystal grew bigger and bigger. The crystal shape after eight days was cubic and after twenty-five days was dipyramidal. It was unclear the evolution from cubic to dipyramidal. One possibility is that the cubic crystal grew larger after prolonged incubation period. Another possibility is that cubic crystals fuesd to yield dipyramidal geometries. In contrast, if the reaction proceeded shorter times, such as two days, unstable Au nanowires formed which could be observed in TEM but were easily burned out by the electron beam. However for three days, Au nanowires were stable enough to maintain their appearance under electron beam, as shown in Figure 2.5(a). The appearance was slightly thinner than four days' incubation in Figure 2.4(d) and the shape was more rod-like instead of rice shape. This demonstrated the Au nanocrystal accumulation behavior on the surface of HRE-coated triple helix template: longer time, more Au attracted and more accumulation;

inhomogeneous Au crystal growth, the middle region of template grew faster than the region of both ends, which could be due to HRE peptide binding to the middle part of triple helix and turning that place into the metal accumulation site of the entire template. The triple helix sequence (shown in Figure 1.3) included some amino acids such as Arg, Glu, Gln which have negative charges or extra polar amide side chain, and this could explain the Au growth and accumulation.

Figure 2.5 TEM images after reduction of HRE-immobilized F877 reacted with Au precursor for (a) 3 days, scale bar 40 nm; (b) 8 days, scale bar 200 nm; (c) 25 days, scale bar 500 nm, all followed with electron diffraction patterns.

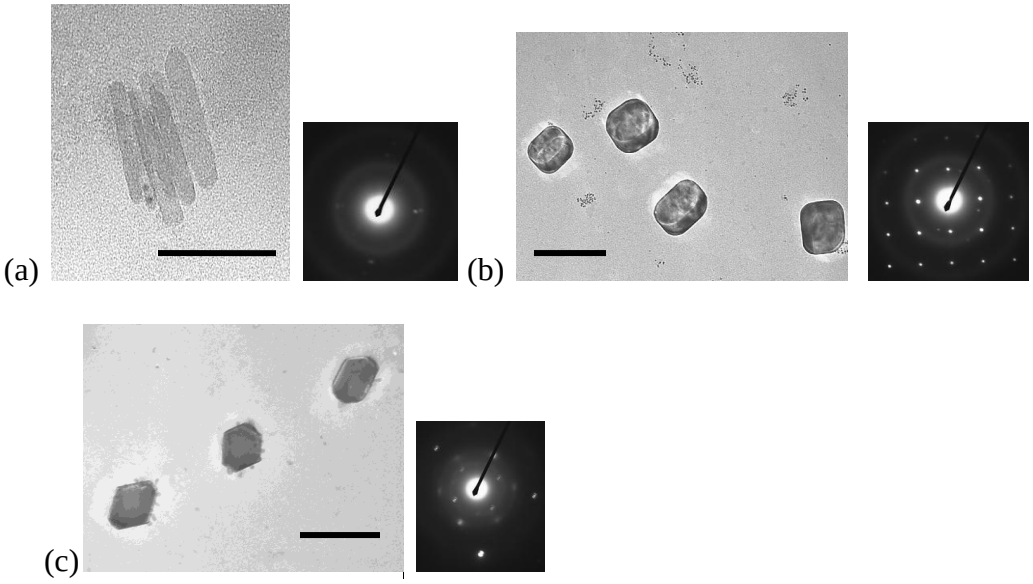

Conclusion

In summary, it was the first trial on utilizing recombinant collagen-like triple helix protein as biotemplate to make nanofabrications. Monodisperse Au nanowires with defined dimension of 4 nm x 40 nm were successfully obtained templating recombinant collagen-like triple helices from an *E. coli* expression system under condition of pH 8.6 . Furthermore, the kinetics of Au nanocrystal growth on template was studied to find out the optimized reaction time length, and the most rigid template of F877 was preferred for future nanowire fabrication. The length of the nanowires can be easily controlled by the number of amino acid residues, and the production of triple helix can be scaled up by means of the cell multiplication. Therefore, the unique molecular properties of collagen-like triple helix combined with the versatility of the recombinant technology offer a promising system to create biomolecular nanowires by design.

Chapter 3. Fabrication of Silver Nanowires in Uniform Size by using Genetically Modified Collagen-like Triple Helix Protein F877 as Template

Nanocrystals have been studied extensively due to their tunability in electronic structures by adjusting their shapes, which naturally leads to significant interest in developing them as building blocks in catalytic, optical, and electronic applications. Biomolecular nanowire templates have shown great potential to serve as excellent building blocks for electronic and sensor devices because of their molecular recognition and catalysis functions. It is essential to satisfy with the critical requirements in the fields of rigidity, monodispersity, and mass producibility. Control of size, shape and size-distribution was achieved by applying specific peptide that had selective affinity for to certain metal or semiconductor and had ability to trap, catalyze and transfer correspondent ions into expected nanocrystal coating onto the template.

Inspired by the idea from nature where various shapes of nanocrystals are produced accurately and reproducibly in biological systems, we developed a strategy to make uniform Ag crystal nanofabrication by introducing specific peptide AG4 and HRE which have silver metal affinity and mineralization capability to pre-coat on the surface of target templates and anchoring Ag precursor via biological recognition. The AG4 peptide (Asn-Pro-Ser-Ser-Leu-Phe-Arg-Tyr-Leu-Pro-Ser-Asp) was found to recognize and effect the Ag nanocrystal growth on the (111) face via the combinatorial phage display peptide library[110] and HRE (Ala-His-His-Ala-His-His-Ala-Ala-Asp) was a histidine-rich peptide and implicated in the biomineralization of heme[111]. Our past studies showed there were successful applications of these two peptides for biomineralization of Au and Ag on the C7 peptide self-assembled nanotubes in which HRE got uniform Au nanocrystals coating

[13, 112]and AG4 got hexagonal Ag nanocrystals coating[113]. When the peptides were incorporate onto the surface of nanotube templates, the binding sites would function as anchoring centers to capture metal ions coming from precursors onto the surface of templates and make them mineralize. The metal nanocrystal growth could be controlled by pH and reaction time length. Finally the nanotubes coated with monodispersed metal nanocrystals in terms of size and shape were achieved and they had potential to serve as building blocks in optics, electronics, and sensor devices[13, 112, 113]. This strategy has an advantage that it does not require the self-assembling process of nanocrystals to organize them into the device configurations since the shape-controlled nanocrystals are grown directly on surfaces and the recognition of the crystalline face with the used peptide is more specific than organic surfactants and other methods. In addition, the less soluble precursors were used because the template and the peptide stayed in solution and precursors sink at bottom, which made them easy to separate by a simple procedure such as centrifugation and then the reaction could be easily controlled[9]. It is highly recommended to use less soluble Ag precursors in the fabrication on the collagen-like protein template.

A similar strategy as in the Au case was employed to fabricate monodispersed Ag nanowires. Three Ag precursor candidates, silver acetate (AgAc), silver chloride (AgCl) and silver nitrate ($AgNO_3$) were assayed. Different pH values were examined with these three precursors which are shown in Table 3.1. The results proved that insoluble or hard-soluble precursor were better than the soluble ones to make the nanofabrication in the Ag case as well as Au case[13]. The explanation was that very little amount of metal ions were released from the salts having very low *K*sp and the concentration of dissociative metal

ions was kept at very low level while these ions were captured and consumed in the biomineralization process which would generate an ideal well-controlled ion environment for metal nanocrystal growth on the biotemplates[13, 114]. Since unreacted metal precursor was continuously removed only by biomineralization process, a lower level of metal ion was maintained, which avoided the formation of metal crystals from the process other than biomineralization. After the reducing reagent was added, the metal crystals formed only from the ion coating onto biotemplates. On the contrary, a soluble salt such as $AgNO_3$ was unable to keep a relative low concentration of metal ions and a large amount of unreacted precursor existed in solution. This is hard to isolate from the biotemplate, and interfere with the fabrication because the nanowire products were affected by large metal crystals coming from unreacted metal ions.

Table 3.1 Harvest of Ag nanowires from three different Ag precursors on different pH conditions in terms of two specific peptides

# of nanowire per grid square	AgAc		AgCl		$AgNO_3$
	HRE	AG4	HRE	AG4	
pH 10.0	n/c	n/c	~18	n/c	n/c
pH 8.6	~20	~6	~40	n/c	n/c
pH 7.0	n/c	~15	~14	~16	n/c
pH 6.0	n/c	~12	n/c	~5	n/c

Experiment section

According to the protocol of Au coating case previous, the first step was mixing the triple helix protein template with specific peptide solution in order to form complex via hydrogen bonding, then adjust the pH and temperature to certain values, the second step was letting the complex anchor and mineralize the ion precursor in a certain time length, the last step was separating the unreacted precursor and product and harvesting the final product by reducing metal ions.

We pre-coated the triple helix with these two peptides, Ala-His-His-Ala-His-His-Ala-Ala-Asp (HRE, GenScript Co.), which has a high affinity for to organic Au or Ag salts [9, 115] , and Asn-Pro-Ser-Ser-Leu-Phe-Arg-Tyr-Leu-Pro-Ser-Asp (AG4, GenScript Co.), which has the ability to recognize certain Ag crystalline face and control the growth of Ag crystal[110, 113] ,separately. 100 μl of F877 triple helix solution (0.5 mg/ml) was mixed with 17.7 μl of HRE solutions (0.1 mg/ml) or 22 μl of AG4 solutions (0.07 mg/ml) as molar ratio of 1:1. Then the pH was adjusted to four different values of 10.0, 8.6, 7.0 and 6.0 separately by adding 0.2 mol/ml Tris buffer solutions and the mixture stayed for one day at 4 ℃. After immobilization of peptides we added 1.0 mg of silver acetate (AgAc, Sigma Co.) or silver chloride (AgCl, Sigma Co.) as precursor into the solution and let them react at 4 ℃. Because these two precursors easily decompose under light, we fully covered the entire reaction container with aluminum foil paper and the entire experiment operation was performing under weak light environment. After reacting for four days the supernatant of the solution containing non-bond Ag salts was removed by a pipette and 2 μl of hydrazine hydrate (Sigma) was added to reduce Ag salts on triple helix complex. After one day's reduction, the solutions became light brown yellow. All

the results including complex of F877 with HRE/AG4, Ag-coated HRE-F877 result and Ag-coated AG4- F877 result were tested by transmission electron microscope (TEM) in dry state. The complex samples were first negative stained by 2%wt of uranyl acetate ($U(OAc)_2$) staining reagent and then prepared on carbon-formvar-film copper TEM grids and the excess solution was dried with a piece of filter paper. The Ag-coat samples were prepared on the carbon-film nickel TEM grids and dried with a piece of filter paper touching the edge of the grids. The images were taken with a Zeiss EM 902 TEM at an acceleration voltage of 80 kV and electron diffraction patterns were obtained with a JOEL 1200 EX TEM at an acceleration voltage of 100 kV.

Results and Discussions

As shown in Figure 3.1 (a), after F877 triple helix protein was coated with AG4 peptide, the width of the whole complex became thicker than the neat F877 protein due to the relative bigger size of AG4 peptide compared to the HRE case (shown in Figure 2.2(b))[110]. From Table 3.1, we knew that pH 8.6 had the best yield of Ag nanowires for the HRE case and pH 7.0 had the best yield for AG4, so two TEM images from AG4(pH 7.0) and HRE(pH 8.6) were selected and shown on Figure 3.1 (b) and (c). All Ag nanowires had monodispersed size in 40 nm of length and 4 nm of width, which was consistent with result of the previous study on Au nanowires in Chapter 2. It proves that this artificial collagen-like triple helix F877 protein was a reliable biotemplate to make monodispersed size nanofabrications and the protocol of pre-coating certain metal-affinity-and-mineralizing peptide was an approved strategy to obtain uniform crystal growth. Since the collagen-like triple helix protein F877 had the virtues of monodispersed length and width that was only determined by the amino acid sequence on

triple helix domain, the size distribution of Ag nanowires product was controlled by the morphology of the protein template. Mutation or modification of the amino acid sequence on triple helix of template would regulate the size of future nanowires. Although both peptides generated a uniform size nanowire product, on the other hand, we could see subtle differences in nanowire appearance between AG4 case and HRE case. In AG4 case the nanowires appeared rice-like oval shape and in HRE case the shape was rod like. These were possible due to differences in inhomogeneous coating of the peptide on the triple helix protein. Although we could not locate the binding site of the peptide on the triple helix, we could observe differences in crystal shape induced by the peptides [110, 111, 113, 116], as it will be discussed later.

To study how the pH condition affects the Ag nanocrystal formation, from our previous studies of these two peptides on C7 peptide nanotubes, the HRE peptide yield Au nanoparticles coating in the pH range from 4 to 11.5 [91] and the AG4 peptide yield Ag hexagonal nanocrystals coating in the range from 4 to 10 [96]. The pH had a significant effect on the metal Au/Ag nanocrystal growth [13, 112, 113]and the packing density of nanocrystals on the template increased as long as the pH value increased, and vice versa. Since both peptides had isoelectric pH (pI) around 6.0 (AG4 at 6.09 [110] and HRE at 6.5 [111]), at pH value higher than 6.0, more negative net charges were carried by the peptides and thus stronger electrostatic attraction for the Au/Ag cation. In HRE case, in general the metal ions bind amine sites of peptides in the pH range between 7 and 10[117], more binding sites were available to anchor Au ions in the higher pH range, and therefore the higher density of the nucleation sites for Au nanocrystals result in the higher packing density of the Au nanocrystals on the nanotubes[13]. In AG4 case, the efficiency of

electrostatic attraction from the amino acids in the AG4 peptide toward Ag ions generally increased as pH increased, and the pH value similar or lower than the AG4 peptide's pI value resulted in relatively slow crystal growth rates that guarantee effective control of shape and size of nanocrystal growth[113]. When we focus onto the pH influence on the packing density of coating Ag nanocrystals, the coating on collagen-like triple helix protein F877 has relatively smaller size compared with C7 nanotubes. Although there was no apparently difference of packing density of coating among various pH values, the pH still influenced the yield of nanowire product. From Table 3.1, regardless of the precursor, HRE case had the highest yield at pH 8.6 and AG4 case had the highest one at pH 7.0, which indicated the optimized pH conditions for the two peptides to acquire the maximum yield of nanowires. And these two pH values for highest yield were inside the pH range of the peptides described above and agreed with the proposed mechanism.

In addition, the solubility of precursor affected the binding reaction of Ag ion and the consequent crystal growth. Although both precursors, silver acetate (AgAc) and silver chloride (AgCl), are hard to dissolve in the aqueous solution, the former can dissociate much more Ag ions than the latter (solubility of AgAc: 11 gram/liter water and AgCl: 0.0019 gram/liter water) and apparently more Ag ions would be available when the reaction took place. More Ag ions resulted in more Ag accumulation on the template and more crystal growth, which definitely influence the shape and size of the crystals. After comparing all TEM results on these two precursors, we found that AgCl had higher nanowire yield than AgAc, the highest yield presented in AgCl case and more bulky crystals showed up in AgAc case than in AgCl case, which confirmed our hypothesis on precursor. Similar as the influence precursor on the reaction, because of the different

binding rates of HRE and AG4, in the same reaction time the higher one would induce bigger Ag nanocrystals growth on the template than the lower one, and therefore fast growth of crystals definitely has an impact on the shape and size. Eventually the aggregation of crystals with out-of-control size would appear instead of nanowires with uniform size. We can conclude that HRE peptide has higher binding rate than Ag4 peptide because higher nanowire yield exhibited in HRE than in AG4 under the same precursor and the same reaction time, which is consistent with the result in Table 3.1. Furthermore the subtle shape variations of nanowires would be the possible consequence of the different growth rates from HRE's and AG4's effects. Within the same incubating time, the HRE having relatively higher binding rate generated rod-like shape uniform width nanowires rather than the rice-like shape product from AG4.

Figure 3.1 TEM images of F877 triple helix protein (a) coated with AG4 peptide; (b) complex of (a) coated with Ag, followed by the electron diffraction pattern; (c) F877+HRE complex coated with Ag, followed by the electron diffraction pattern. Reaction condition (AG4 in pH 7.0 & HRE in pH 8.6). Scale bar 50 nm.

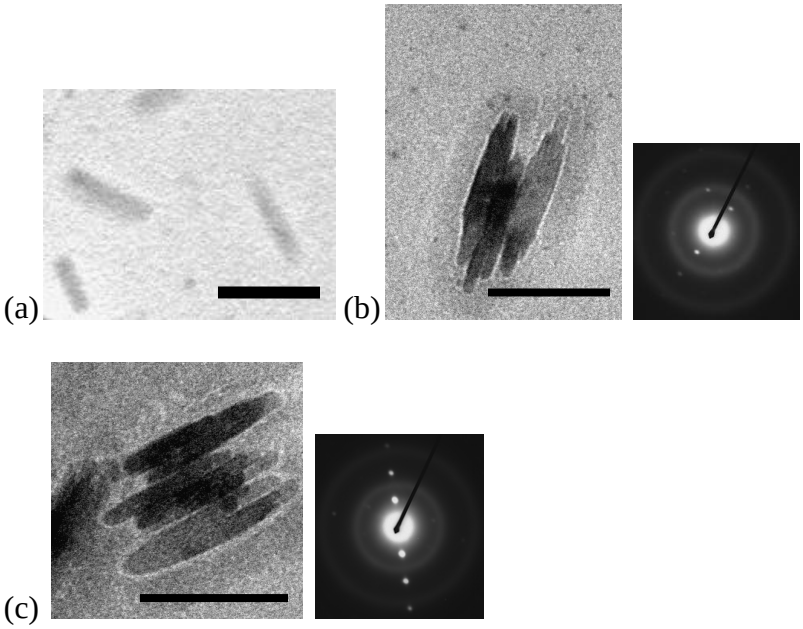

Conclusion

In summary, similar to Au nanowires in Chapter 2, monodisperse Ag nanowires with uniform dimension of 4 nm x 40 nm were achieved by utilizing the biotemplate of recombinant collagen-like triple helix protein F877 coming from an *E. coli* expression system. The length of the nanowires can be easily controlled by the number of amino acid residues. Two metal-affinity-and-biomineralization specific peptides, HRE and AG4, were tried on fabricate Ag nanowires. Both peptides had significant influence on the Ag crystal growth and HRE had higher reaction rate than AG4 in the process of Ag ion anchoring and crystal growth. The pH value was essential for the kinetic control of Ag nanocrystal growth and the control of size and shape of nanocrystal product; therefore it would affect the final yield of nanowire. From experiment, the pH values for the best yield of nanowire from HRE peptide was 8.6 and for the one from AG4 peptide was 7.0. The precursors were also important for the yield because the Ag salt having less solubility was observed to obtain higher yield. The pH value and the selection of precursors would be the base for future nanowire fabrication used as building blocks in developing catalytic, optical, and electronic devices or sensors.

Chapter 4. Low Temperature Synthesis of ZnO Semiconductor Nanowires by using a Genetically Modified Collagen-like Triple Helix F877 as a Catalytic Template

Introduction

The recent advancement of nanomaterial synthesis can be highlighted into two features: low temperature synthesis and controlled dimension. For example, most of the important oxide semiconductor nanowires are synthesized at high temperature for electronics and the low temperature synthesis will be effective to reduce energy consumption in manufacturing processes since it will decrease the production cost, the facility size (such as cooling systems), and the manpower if these syntheses can be conducted in low temperature[118]. In order for the high quality control of the assembled devices, the size monodispersity of the building blocks such as semiconductor nanowires is also critical in their practical applications. Therefore, uniformity in size and shape and the low temperature growth process are two key areas needed to be addressed for the advanced semiconductor nanowire synthesis, but unfortunately no material synthesis method scores high on both features.

Nature tends to find the easiest way to grow materials with high efficiency and high selectivity in dimension and shape at room temperature, which our conventional chemical synthesis method cannot match[8]. Biomimetic approach is a potential path to break through this challenge because biocatalytic function of biomolecular nanowire templates exhibits high efficiency and accuracy in the material growth at room temperature or even lower temperature. Recently biomolecular nanowires were demonstrated be promising biomimetic building blocks to template metal growths[80, 81, 83-91, 93, 94, 119-122] . However, a

disadvantage of these biomolecular nanowire templates is the lack of conformational rigidity. For example, the tendency of supertwisting of the double-helix DNA structure makes it difficult to obtain rigid and straight nanowires. The structural stability is also necessary for the proposed semiconductor coating process on biomolecular nanowire templates; generally, biomolecular nanowires have difficulty in serving as templates for semiconductor coatings since they are not stable enough to survive in the severe semiconductor growth environment such as extreme pH, solvent, and strong reducing environment.

Here we developed a new biomimetic method to grow crystalline oxide semiconductor nanowires by using the genetically-modified collagen triple helix peptide nanowire as a mechanically-improved bionanowire template. This bio-templating method could address both needs for practical semiconductor nanowires; low temperature synthesis and monodispersity in size for resulting semiconductor nanowires. Collagens are the major components of extracellular matrices for bones, cartilages, skins, blood vessels and corneas. We targeted this biological nanowire as a template for monodisperse ZnO semiconductor nanowire growth since they are the most abundant proteins in higher organisms with superior mechanical properties[100-102]. Other advantages using this collagen-based triple helix peptide are that this biomolecular nanowire is monodisperse in both diameter and length and their dimension can be controllable; the length of the triple helix nanowire is determined by the number of amino acid residues in the triple helix, controllable with the well-established recombinant technology[3, 9]. It is also advantageous that for the mass production triple helix peptide can be amplified by the cost-effective *Escherichia coli* (*E.coli)* expression system. In this chapter, we modified the sequence of

wild type collagen triple helix peptide with the recombinant technology to increase the mechanical rigidity. Due to the enhancement of the mechanical strength, our triple helix peptide was stable in the severe ZnO growth condition and yielded the single crystalline ZnO nanowires successfully. The addition of synthetic peptide to the triple helix that has a high affinity for to zinc precursor could catalyze the crystal growth of ZnO below room temperature.

In this study, the low-temperature growth of ZnO on the triple helix peptide, which has a wide band gap (3.37 eV) and possesses unique optical, acoustic, catalytic, and electronic properties, was examined as a model system for the oxide semiconductor nanowire synthesis[123-126] . While recently various methods were published to grow ZnO in various shapes at near room temperature[127-129], there were no reports about controlling the size and the monodispersity of ZnO nanowires at the temperature lower than room temperature. Our approach here is to use the monodisperse biomolecular nanowire, which incorporates a peptide sequence catalyzing ZnO growth below room temperature, as a template to growing ZnO in the nanowire shape in the uniform diameter and length. Although the wild type collagen triple helix is made of three polypeptide chains tightly twisted and bundled together to form a rigid, rod-shaped molecule, it was necessary to further improve their rigidity by modifying their sequence with the recombinant technology because ZnO nanocrystals need extremely high pH to be grown at low temperature and the wild-type collagen triple helix was not rigid enough to survive in this environment. The high pH growth media was reported to favor condensation and dehydration of the intermediate zinc hydroxide to produce zinc oxide[130-133]. Previously we attached the gold-mineralizing peptide on the surface of F877 triple helix via

hydrogen bonding[3], in this work we used the same strategy to attach a synthetic peptide, ZnO-1 (Glu-Ala-His-Val-Met-His-Lys-Val-Ala-Pro-Arg-Pro-Gly-Gly-Gly-Ser-Cys), which has a high affinity for to ZnO crystals and catalyzes ZnO growth at room temperature[125]. It appeared no significant changes in length, diameter, and shape after the complexation of the F877 triple helix with the ZnO-1 peptide (Figure 4.1(a))[4].

Experiments

To grow ZnO nanocrystals on the F877 triple helices, we mixed 80 μl of F877 solution (0.5 mg/ml) with 55 μl of ZnO-1 peptide solution (0.1 mg/ml) for the molar ratio of 1:3. To increase the molar ratio of the ZnO-1 peptide ten times with respect to the F877 triple helix, we also prepared 55 μl of 1.0 mg/ml ZnO-1 peptide and mixed with 80 μl of F877 solution (0.5 mg/ml). These mixtures were vortexed for 10 seconds and left for 1 day at 4 ℃. The ZnO-1 (Glu-Ala-His-Val-Met-His-Lys-Val-Ala-Pro-Arg-Pro-Gly-Gly-Gly-Ser-Cys) was purchased from GenScript Co., NJ. To adjust pH of the solution, we added 300 μl of 0.2 mol/l Tris buffers in pH 4.0, 7.0, 8.0, 10.0, respectively and vortexed for 10 seconds. After pH of solution was confirmed by pH meter, 4.2 mg of zinc acetate dihydrate ($Zn(Ac)_2 \cdot 2H_2O$, Sigma Aldrich Co.) was added into the solution with respective pH. To minimize the fluctuation of the reaction temperature, we prepared and mixed all peptide solutions and buffer solutions at consistent 4 ℃. After nine days, we centrifuged the solution under 12,000 rpm for 10 minutes and separated 3 μl supernatant to extract the ZnO-coated triple helix peptides. The supernatant was dropped onto carbon-coated nickel TEM grids and the excess solution was dried by filter papers. The dried TEM grids were then examined with a Zeiss EM 902TEM at acceleration voltage of 80 kV for low-resolution imaging. HRTEM of the samples was imaged with a FEI Tecnai

20 at the acceleration voltage of 200 kV. The electron diffraction patterns and energy-dispersive X-ray spectroscopy (EDX) were taken with a JOEL-TEM2200F. Simultaneously, we performed a control experiment without F877 triple helix in which we incubated the same amount of ZnO-1 peptide with the same amount of $Zn(Ac)_2 \cdot 2H_2O$ precursor for nine days and harvested the results in the same procedure. Moreover, the results were tested with the same TEM.

Figure 4.1 (a) TEM image of the F877 triple helix peptide with the ZnO-1 peptide (EAHVMHKVAPRPGGGSC) on its surface; (b) TEM image of ZnO nanowires grown on the ZnO-1-F877 triple helix peptide complexes at pH 10.0 and 4 ℃, (c) Elemental analysis of (b) by energy-dispersive X-ray spectroscopy (EDS), (d) Electron diffraction pattern of ZnO nanowires in (b), (e) HRETEM image of the ZnO nanowire in (b). The spacing of lattice is 2.2 Å.[4]

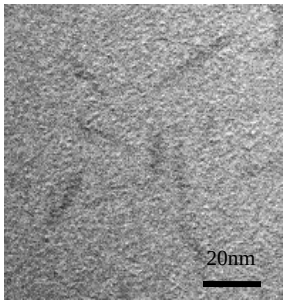

(a)

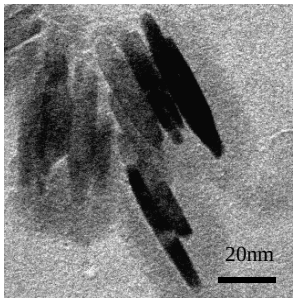

(b)

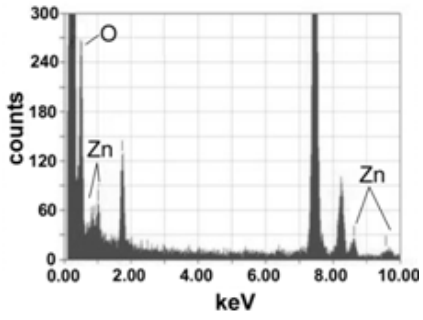

(c)

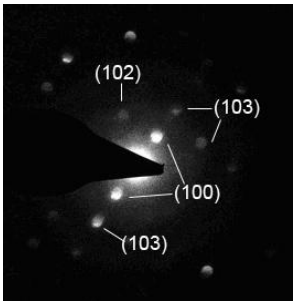

(d)

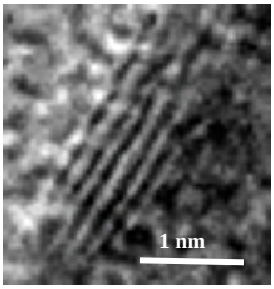

(e)

Results and Discussions

When zinc acetate was hydrolyzed on the F877 triple helix at pH 10.0 and room temperature for nine days, ZnO nanowires were obtained from the supernatant of the growth solution via centrifugation, as shown in Figure 4.1(b). Elementary analysis of these nanowires in Figure 4.1(c) showed that the ZnK_{α} line (8.64 keV), the ZnK_{β} line (9.57 keV), and the oxygen K_{α} line (0.52 keV) were clearly observed in the EDS spectrum of the ZnO coating on the triple helices, and the characteristic band gap of ZnO at 361 nm was also confirmed by its photoluminescence spectrum (shown in Figure 4.3). Electron diffraction pattern in Figure 4.1(d) also matches the (100), (102), and (103) faces of ZnO. ZnO crystals were only grown on F877 triple helix proteins and without the template biomolecular nanowires only amorphous zinc hydroxide aggregates were obtained under the same experimental condition at 4 ℃ (Figure 4.2(a)). We also examined another control experiment to incubate F877 triple helices without attaching the ZnO-1 peptide in the ZnO growth solution and there observed no single crystalline ZnO coatings on the triple helices (shown in Figure 4.2(c)). Since single crystalline ZnO was grown on the F877 triple helices only when the ZnO-1 peptide was attached on the helix surface, the ZnO coating in Figure 4.1(b) serves as indirect evidence that the ZnO-1 peptide is indeed incorporated on the triple helices in Figure 4.1(a) and this peptide is responsible to catalyze the ZnO growth at lower temperature. In order for the generation of highly reproducible results, it was important to keep and mix all solutions including the complex solutions and other buffer solutions at the same temperature of 4 ℃ to prevent the temperature fluctuation generated by the mixing. The size of resulting ZnO nanowire is monodisperse in 4 x 40 nm, the same dimension as the F877 triple helix,

while the coated ZnO nanowire has a rice-like shape and the middle part of wire has thicker ZnO coating, which was also observed previously when the triple helix was coated by Au[3]. The rice-like shape of ZnO nanowire could be originated from the inhomogeneous coating of ZnO-1 peptide at the ends of F877. As shown in Figure 1.3, the foldon at the C-terminal end forms a three stranded β-hairpin propeller, a conformation very different from that of the triple helix; while the helix fray at the N-terminal end of the triple helix domain has been well documented by structural studies of crystallography and NMR[106]. These conformation differences likely resulted in different binding of the ZnO-1 peptides and leading to less ZnO growth on those ends as compared to the well-ordered middle part of triple helix, consistent with the rice-shape formation. Since the wild-type collagen ruptured and disappeared under the same growth condition, this result demonstrates that the recombinant collagen-like triple helix improved its structural stability strong enough to survive under the extreme base growth condition. The same growth condition at pH 8.6 also produced the ZnO nanowires but the yield was 50% lower and the rest of product was amorphous zinc hydroxide nanoparticles. When the solution of pH was reduced lower than pH 8.6, no ZnO nanowires were observed. The high-resolution transmission electron microscopy (HRTEM) revealed the lattice fringe of the (103) face of the resulting ZnO nanowire and this observation indicates that this ZnO nanowire is highly crystalline (Figure 4.1(e)) and ZnO crystallization along the long axis of the tripe helix occurred in the direction perpendicular to this crystalline face.

Figure 4.2 TEM images of (a) the solution containing the ZnO-1 peptide and zinc acetate at pH 10.0 and 4 ℃, (b) the ZnO-1-F877 triple helix nanowires at pH 10.0 and 4 ℃ when the concentration of the ZnO-1 peptide was increased 10 times more than the concentration in Figure 4.1(b), (c) the neat F877 triple helices without the ZnO-1 peptide after mixing with the ZnO precursor solution at pH 10.0 and 4 ℃. Inset is the electron diffraction pattern matching $Zn(OH)_2$ (from center to outer, (111), (022), and (310)).[4]

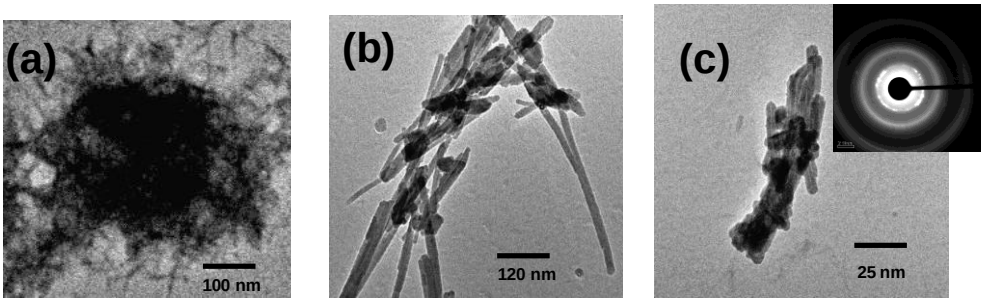

Figure 4.3 Photoluminescence spectrum of the triple helix protein F877-templated ZnO nanowires. The characteristic band gap of ZnO at 361 nm was confirmed by its photoluminescence spectrum[4].

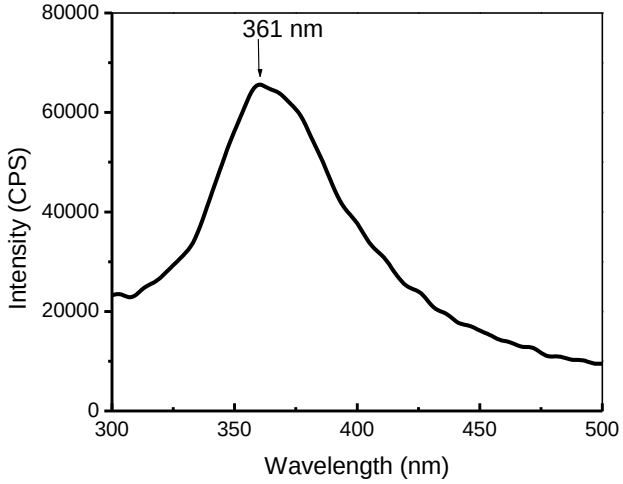

Monodisperse ZnO nanowires in Figure 4.1(b) were obtained when the triple helix and the ZnO-1 peptide was mixed in the 1:3 molar ratio before the ZnO precursor was added. When the concentration of ZnO-1 peptide was increased to 10 times from the original concentration and the same amount of ZnO precursor was added to the solution, larger nanowires with no ZnO coating were observed (Figure 4.2(b)), whose size was 40 nm x 400 nm. The high concentration of ZnO-1 peptide induced the aggregation of F877 triple helix and the aggregated template did not catalyze the dehydration of zinc hydroxide even at pH = 10.0. This result indicates that the excess amount of the ZnO-1 peptide could bundle these triple helices with the assistance with zinc ions, resembling the formation of collagen fibrils from triple helices.

Previously, it has been reported that zinc ions form the intermediates, $Zn(OH)_x(OH_2)_{6-x}$ in the extreme high pH condition, and the condensation of these complexes with elimination of water yields ZnO crystals[130]. The growth and the crystallinity of ZnO are dependent on how these intermediates are effectively precipitated and condensate to undergo the dehydration reaction[132]. Here we hypothesize that the ZnO-1 peptide plays an important role to grow single crystalline ZnO at this extreme condition, and thus we examined whether ZnO can be grown without the ZnO-1 peptide. When the neat F877 triple helix was incubated in the ZnO growth solution under the same condition, the resulting nanowires in Figure 4.2(c) looked similar to the ZnO nanowires in Figure 4.1(b), however the electron diffraction pattern (inset, Figure 4.2(c)) showed that these nanowires were coated by $Zn(OH)_2$. Thus, this control experiment showed that the F877 triple helix without the ZnO-1 peptide failed to catalyze the growth of crystalline ZnO. Previously, Umetsu et. al. reported that cysteine in GGGSC tag of the

ZnO-1 peptide was required to grow flower-like ZnO microparticles at room temperature[125], and the combination of this GGGSC tail and the rest of amino acid residues, EAHVMHKVAPRP, is likely important to grow single crystalline ZnO nanowires at low temperature and pH 10.0; At pH 10.0, cysteine is charged negatively and this negative charge recruits positive zinc ions onto the template nanowires efficiently. Then, the basic amino acid-dominant EAHVMHKVAPRP part could produce local pH and charge distribution in molecular level that favors the condensation of the intermediates and catalyzes the dehydration to produce ZnO[125, 134, 135]. Cysteine in the tail could have an additional role to hydrolyze hexaqua zinc into the intermediate $Zn(OH)_x(OH_2)_{6-x}$ effectively and slow the condensation reaction which favors the single crystal formation on the F877 nanowire [133, 136]. The local environment is sensitive to the conformation of the mineralizing peptide, and the ZnO-1 peptide seems to have a ideal geometry on the triple helix for the single crystalline ZnO growth below room temperature.

Conclusion

Mmonodisperse and single crystalline ZnO nanowires were grown by using collagen-like triple helix peptides as templates at pH 10.0. The conjugation of the zinc-mineralizing ZnO-1 peptide onto the triple helix catalyzed the growth of single crystalline ZnO below room temperature since the peptide optimized local pH environment and charge distribution at the peptide interface for the catalytic activity. Another technological impact from this report is to introduce a strategy to produce rigid biomolecular nanowires that can be stable at severe reaction conditions. In general, biomolecular nanowires are not stable enough to serve as templates for the semiconductor

growth under high pH condition and strong reducing agents, but we could overcome the rigidity of the triple helix nanowires by modifying its sequence via the recombinant technology. This triple helix peptide with the improved structural stability could be functioned as a template even in the extreme base condition and yield crystalline ZnO. This approach will enable one to produce various semiconductor and metal nanowires using the peptide nanowires as templates, which requires the extreme growth condition. The development of biomimetic process to produce monodisperse ZnO nanowires with well-defined length and diameter is also critical achievement in this work. It is advantageous that our biomimetic method can produce semiconductor nanowires in the uniform dimension because the length of the template is determined by the number of amino acid residues of the peptide and the recombinant technology will allow one to control the length of the nanowire template between 40 and 300 nm.[3]

Chapter 5. Low Temperature Synthesis of Titanium Dioxide Semiconductor Nanowires by using a Recombinant Collagen-like Triple Helix F877 as a Catalytic Template

Introduction

Titanates are well-known as functional ceramic materials (dielectric, piezoelectric, ferroelectric, and low absorption of infrared radiation),[137-140] and titanate-fibers are widely used as structural reinforcements in polymers, metals, and ceramic-composites[141, 142] because of their outstanding mechanical properties and thermal stability. Moreover, titanium dioxide (TiO_2) is one of the most important metal-oxides[143, 144]. In addition to its well-known use as pigments, these oxides have recently found advanced application as photocatalysts as catalyst supports[145, 146] as materials for converting solar energy into electricity, as gas sensors, and as Li ion battery materials[144, 147-150]. There is also great interest in the development of titanates and TiO_2-based solids with nanoscale dimensions and high morphological specificity,[137-139, 149-162] such as nanofibers[150], nanosheets[152, 153], and nanotubes[154] because of their demonstrated potential in solar energy conversion[155], photocatalysis[144, 153, 156, 163, 164], photovoltaic devices[151, 165, 166], and carrier for metallic nanoparticles[167, 168]. Moreover, these nanostructures have the potential to exhibit unusual properties and offer the opportunity to investigate physical and chemical processes in size-confined systems[143]. The structure and resulting physical and chemical properties of these nanostructures are size-dependent and cannot be determined by extrapolation of bulk characteristics[169]. For instance, TiO_2 and titanates are generally “refractory” mineral substances in bulk form and have good chemical and thermal stability[139, 152-154, 170].

There were numerous studies about the synthesis of titanium dioxide nanowires or nanofibers because TiO_2 especially in the anatase structure has been used as an excellent photocatalyst for photodecomposition and solar energy conversion due to its high photoactivity [171, 172], which was very important for the energy and environment conservation [173, 174], and many processing methods were developed. For example, sol-gel synthesis method[175-178], hydrothermal treatment[179], electrospinning[180], electrodeposition[181], templating processing[182], and phase transition processing[143] were tried and hollow/mesoporous nanotubes or solid nanowires/fibers/rods were successfully achieved. However, accurate controlling of size and shape and conducting of expected crystal structure were not easy. For instance, sol-gel method was a versatile process that made precursors to hydrolyze and polymerize, in general amorphous structure nanowires or nanofibers were obtained and the size distributions were in a wide range[174]. What is more, the operation temperatures for most fabrication methods were normally much higher than room temperature, which increased the energy cost apparently. Templating on biomolecules such as specific protein/peptide is a prospect way to fabricatie size-controllable and rigid nanowires because biotemplate that has both biorecognition and biocatalysis functions can affiliate to the precursor, convert to expected crystal structure products more efficiently than normal inorganic processing method via biomimetic process and fabricate nano product in biomineralization. In nature, biomineralization processes take place at room temperature or lower. Inspired by nature, similar process templated by biomolecules could be performed at room temperature or lower condition in order to save energy.

Here we introduced the collagen-like genetically modified F877 protein as biotemplate to make TiO_2 nanowires with monodispersed size-distribution. After a specific peptide Arg-Lys-Leu-Pro-Asp-Ala-Pro-Gly-Met-His-Thr-Trp (Ti-RK)[183-185] was bound on the surface of the template via hydrogen bonds, the complex formed that had the ability to capture the titanium ion from the precursor and catalyze the condensation and dehydrolysis of titania on its surface. The artificial recombinant collagen-like F877 protein molecule is a monodispersed and rigid biotemplate due to its collagen-like homogeneous triple helical trimer forming from three identical monomer chains. These monomers are mainly composed of a sequence identical to part of original collagen I α1 chain and strengthened by incorporating with cysteine knots, a foldon and two sets of repeating tripeptide (Gly-Pro-Pro) combination units.

Our past study indicated that the Ti-RK peptide had high affinity for Ti, Si and Ag surfaces[183] and could be utilized as Ti-binding peptide to anchor the Ti precursor onto the surface of C7 nanotube template and transfer Ti ion to TiO_2 nanocrystal coating on the template[184]. The size of TiO_2 nanocrystals could be controlled by pH condition and incubation time. Inspired by this idea, we tried to set up this procedure to make TiO_2 nanowires templating triple helix protein F877, first precoating Ti-RK peptide onto F877, second incubating with suitable Ti precursor, and then harvesting TiO_2 nanowires. Simultaneously we discovered another Ti/Zr affinity peptide Zr-A (Ser-Gly-Gly-His-Gly-Gly-Arg-Gly-Gly-His-Phe) coming from combinatorial peptide library[186] and run similar procedure with Ti-RK peptide in parallel.

Experiments

We made two Ti-affinity peptides solutions, 4.3 μl of Ti-RK (RKLPDAPGMHTW, GenScript Co., 0.36 mg/ml), and 2.4 μl of Zr-A (SGGHGGRGGHF, GenScript Co., 0.48 mg/ml), and let them mix with 80 μl of F877 triple helix protein solution (0.5 mg/ml) in the molar ratio of 1:1 in eppendorf tubes, separately, and incubate them for 1 day under 4 ℃ condition. Then we adjusted pH to 7.0 and 9.0 with 250 μl of 0.2 mol/l Tris buffers, added 1.5 μl of titanium isopropoxide precursor ($Ti(O\text{-}isoPro)_4$, Sigma Co.,10 % wt, diluted by isopropanol) to the two incubated solutions individually. We could observe a white precipitate immediately after adding the precursor. Then we incubated them at 4 ℃ to slow down the hydrolysis rate and maintain the structure of triple helix. Because of the affinity difference of the two peptides, we set up different reaction times as two days, five days and seven days to find the ideal time length for them. Subsequently, the reaction tubes were centrifuged for three minutes at 12000 rpm. Then 4 μl of the supernatant were picked up, the TEM samples were prepared by dropping solutions onto carbon-coated nickel TEM grids and drying the excess solution by filter papers. The dried TEM grids were then examined with a TEM (Zeiss EM 902) at acceleration voltage of 80 kV for imaging and the electron diffraction pattern was acquired with a JOEL 1200 EX TEM at an acceleration voltage of 100 kV.

Results and Discussion

Without the effect of Ti-affinity peptides, the reactions between aqueous soluble template and organic titanate precursors will be vigorous which could result in the rupture of triple helix protein. Compared with the reaction in Zn precursor of Chapter 4,

the reaction in Ti was more severe and the Ti precursor was more active even though we pre-dilute it to slow down the whole reaction.

After binding with specific peptides via hydrogen bonding, the triple helix protein F877 could produce TiO_2 nanowires with uniform size and shape as shown in Figure 5.1 (a & b) and yields varied in terms of peptide, pH and reaction time length. For Ti-RK peptide, the TiO_2 nanowires showed the best yield in pH 7.0 and two days' reaction time. From Figure 5.1(a) the rod-like nanowires showed dimension of 40 nm $\times$ 5 nm and the diffraction pattern indicated the anatase crystal structure which could be estimated by comparison with Al standard diffraction pattern. If the incubation time was longer such as seven days, bulky TiO_2 crystal (shown in Figure 5.1(c)) would form via fusion of many TiO_2 nanowires of Figure 5.1(a). The possible explanation was mutual alignment of identical crystal face among these uniform-size TiO_2 nanowires existed while TiO_2 continued growing on the surface of nanowires, which resulted in nanowires connecting to each other, fusing and transforming into much bigger size crystals [187, 188]. Sufficient time could make bulky crystal attract more nanowire and this was indicated by the single nanowire with defined dimension close to bulky crystal shown in Figure 5.1(c) inset. For Zr-A peptide, there were no nanowires observed after two days or five days reaction regardless of pH and nanowires appeared after seven days at pH 9.0. The yield was lower than the best yield of Ti-RK peptide. This could be explained by the higher pI (isoelectronic point) of Zr-A above 9.0, which required high pH to make the peptide contain more negative and attract Ti ion from the solution. Higher pH generated more $Ti(OH)_4$ compared with lower pH [179],which resulted in weaker dehydrolysis, consequently less TiO_2 product were obtained. On the contrary, Ti-RK had pI of 8.0

which could bind Ti efficiently at lower pH around 7.0, which enhanced the binding on the template and more yield was obtained. We can conclude Zr-A peptide had less affinity for Ti precursor compared with Ti-RK peptide since it required higher pH to effectively attract Ti ion, and it had less ability to transfer $Ti(OH)_4$ to TiO_2, hence less yield of nanowires compared with Ti-RK peptide. Ti-RK was a much suitable candidate peptide to make TiO_2 nanowires.

Since we successfully achieved anatase nanowires by templating F877 triple helix protein and utilizing Ti-binding peptide under 4 ℃ temperature which was much lower than the process temperature of classical method for making TiO_2 crystal nanowires or nanofibers, this could be a prospective way to make uniform size semiconductor nanowires effectively and economically.

Figure 5.1 TEM image of (a) TiO_2 grown on F877 triple helix coated with Ti-RK peptide followed with electron diffraction pattern, reaction condition: pH 7.0, time 2 days, 4 ℃; (b) TiO_2 grown on F877 triple helix coated with Zr-A peptide, reaction condition: pH 9.0, time 7 days, 4 ℃; (c) TiO_2 grown on F877 triple helix coated with Ti-RK peptide, pH 7.0, time 7 days, inset are HRTEM image of the single nanowire.

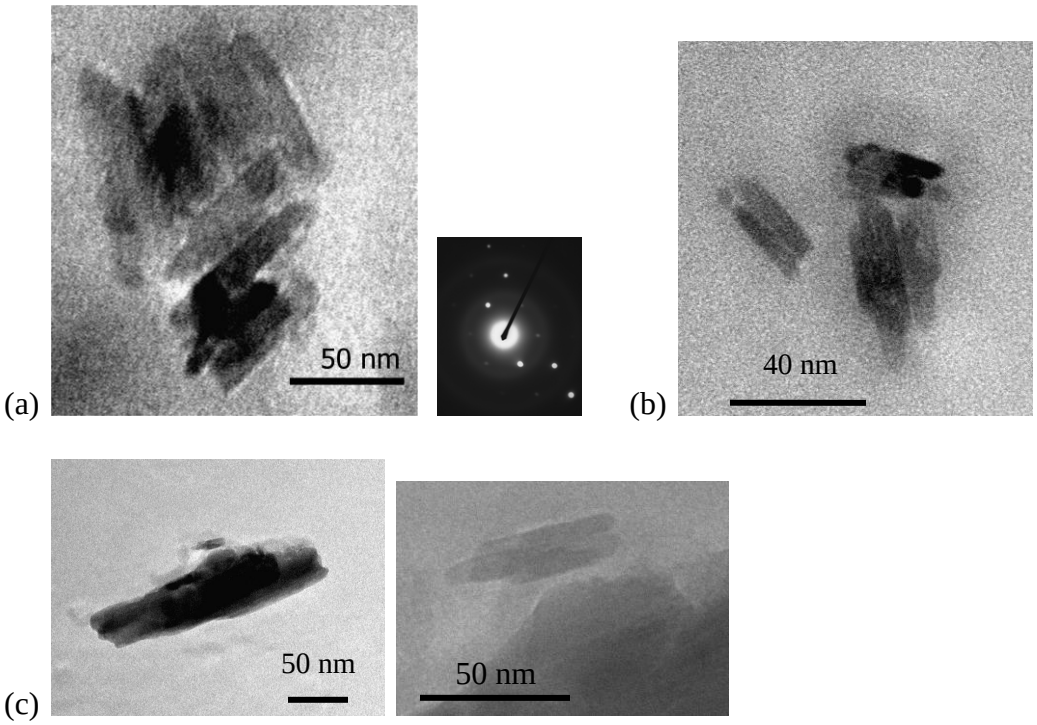

Conclusion

In summary, anatase nanowires with uniform size were achieved by utilizing triple helix template bound with specific Ti-affinity peptide and the advantage of fabrication method was the length of nanowires was determined by the amino acid sequence of triple helix molecules. Ti-RK peptide had the best yield of TiO_2 and could be the best candidate peptide used for future anatase nanowires compared with Zi-A peptide. Practical pH condition and reaction time length were found out based on series of experiments.

Chapter 6. Design and Synthesis of Collagen-like Triple Helix Protein as Monodisperse and Rigid Biomolecule Template to Make Nanofabrication

Introduction

The fabrication of one dimensional nano structures such as nanoparticles and two dimensional nano structure such as nanowires or nanotubules with controllable size or scale have received more and more attention in recent ten years. To make crystalline two dimensional nano-scale materials, biotemplate coating/attaching are one of the methodologies applied, since nature provides plenty of selection of nano-scale materials with characteristic shape and patterns that could be potentially developed as biotemplates for fabrication of a wide range of structural materials. For example, double-stranded DNA[17], F-actin filaments[18], peptide microtubules[19], amyloid fibres[20] and lipid tubules[21] as well as biological organisms (bacteria[22], viruses[23, 24], fungal colonies[25], etc.) have been widely employed as templates to fabricate structural functional inorganic materials. Biotemplates have such merits as biorecognition, biocatalysis, and bioconstruction etc, furthermore biotemplates could attach with other specific peptides, protein or other biomolecules to become multi-functionalized biocomplex to make crystallized nanomaterials.

One example is biomineralization, where peptides or proteins attached to biotemplate are utilized to mineralize metals and semiconductors, which have been demonstrated to produce various types of nanocrystals [19, 26, 189-200]. Since the amino acid sequences are very sensitive to elements for their mineralization, optimized peptide sequences can produce nanocrystals efficiently [112]. In addition to the effective crystal growth, the amino acid sequences of mineralizing peptides could also influence the size, the alignment, and

the shape of resulting nanocrystals [113, 201-203]. Furthermore, in some cases, peptides could mineralize nanocrystals in solution at room temperature that do not grow under the ambient condition [204].

Although biotemplates have such intrinsic advantages in nanomaterial fabrication, there are requirements for them in terms of stability, morphology and production. Especially the critical chemical or physical conditions in crystal growing, the rigidity and stability of biotemplate will be the essential. Collagen type I is a good candidate of biotemplate because collagen type I occupies 90% abundance of all collagen types and it is the major component of extracellular matrix bones, cartilage, skin, blood vessels, cornea and so on [39, 205]. The basic conformation of collagen especially collagen I is a triple helical trimer[55, 62]. In order form triple helical trimer from the three packing chains, the triple helix domain on the chain requires every third residue to be glycine (Gly), as any larger residue here is highly destabilizing, the first and second residue should be (Gly-Xaa-Yaa) combination units. Melting temperature T_m represents the stability of the triple helix part formed by these tripeptide (Gly-Xaa-Yaa) combination units, and each (Gly-Xaa-Yaa) combination unit has its specific value of T_m. The T_m values of all (Gly-Xaa-Yaa) combination units (shown in Table 1.1) could be theoretically calculated or experimentally estimated, there were lots of references about the theoretical or experimental thermal stabilities of triple helix [33, 73, 74] and the values of T_m of different (Gly-Xaa-Yaa) combination units, which could be utilized as reference for the designing of new artificial triple helical conformation protein or peptide in the future.

Past studies showed commercial collagen I proteins could not survive in the critical conditions although its triple helix had 300 nm length[4]. There were studies about

designing and making new artificial triple helical proteins by using recombinant technology. Through recombinant technology, we can create a brand-new artificial collagen-like triple helix protein that should have the properties of monodispersity, rigidity and ability to be easily mineralized metal or semiconductor ions and can, thus, be applied as future biotemplate to satisfy with those critical requirements in making metal or semiconductor nanowire fabrications.

Since in the past we had successful experience in designing and making artificial F877 triple helical protein by recombinant technology, which had a length at 40 nm and was a homogeneous triple helix made from three identical chains each of which included 93 amino acids in its triple helix domain [5, 9], we can use the same strategy to design this new triple helical protein. According to the study on F877, the length of protein was determined only by the sequence of triple helix domain; we were able to control the length of the protein by adding or reducing the codons corresponding to the amino acids of (Gly-Xaa-Yaa) combination units in genetic mutations. To avoid the risk of too long length reducing the stability of entire protein, we set the length of the new triple helix as 90~120 nm, shorter than the 300 nm of normal collagen. Besides the triple helix domain as the backbone of the entire protein, two conformations of protein or peptide, cysteine knot and foldon, were utilized in the recombinant sequence to increase the thermal stability. The foldon domain was coming from bacteriophage T4 fibritin, which serves as the nucleation site for the formation of the triple helix and was widely used in the studies of triple helix protein or peptide in recent years[103, 206]. The cysteine knot is a pair of Cys residues inserted between the triple helix domain and other domains in order to covalently link the three chains of the triple helix through a set of interchain disulfide

bonds. After the genetic modification on conformation, the denaturing temperature of F877 triple helix protein increased more than 5 ℃ as compared to the wild type collagen which indicates the enhancement of the rigidity [9].

Here is the sequence of triple helix domain of 242 protein, as shown in Figure 6.1(a), this domain consists of 3 × 108 amino acid residues modeling the region starting at the position 242 (from the N-terminus, No.242─256, No.296─322, No.434─478 and No.515─535) of the α1 chain of type I collagen, in which all (Gly-Xaa-Yaa) combination units were selected as the ones having higher T_m as possible according to the literature[73]. Four of $(Gly\text{-}Pro\text{-}Pro)_4$ were added at both ends of the 108 residues to increase the mechanical and thermal stability of the triple helix, because the combination of (Gly-Pro-Pro) has almost the highest T_m more than 45 ℃ in all (Gly-Xaa-Yaa) combinations and has no charge [207]. At the ends of the triple helix domain two pairs of cysteine knots were attached and after the knot at C-terminus a foldon domain was included through the monomer chain. A homogeneous collagen-like triple helix protein will form from three such monomer chains by the action of interchain H-bonds, and its stability will be intensified by the interchain disulfide bonds from cysteine knots and foldon.

Figure 6.1 Illustrated structure of triple helix protein 242 fragment.

(a) The triple helix domain consists of three identical parts each of which is the same sequences as No.242-256, No.296-322, No.434-478 and No.515-535 parts on collagen I α1 chain, four of $(Gly\text{-}Pro\text{-}Pro)_4$ were added between these three parts separately.

(b) The gene expression construct of the fragments. The His-tagged and thioredoxin was removed during the last purification procedure by thrombin digestion at the cleavage site APR.

(c) The restriction endonuclease sites of the three DNA pieces. These three pieces were synthesized separately, then connected by restriction enzymes to make the complete DNA sequence for 242 triple helix protein. From 5' to 3', first part and second connected by XbaI, and second and third by KpnI. The complete DNA sequence was bracketed between BamHI site and EcoRI site on pET32a(+) vector.

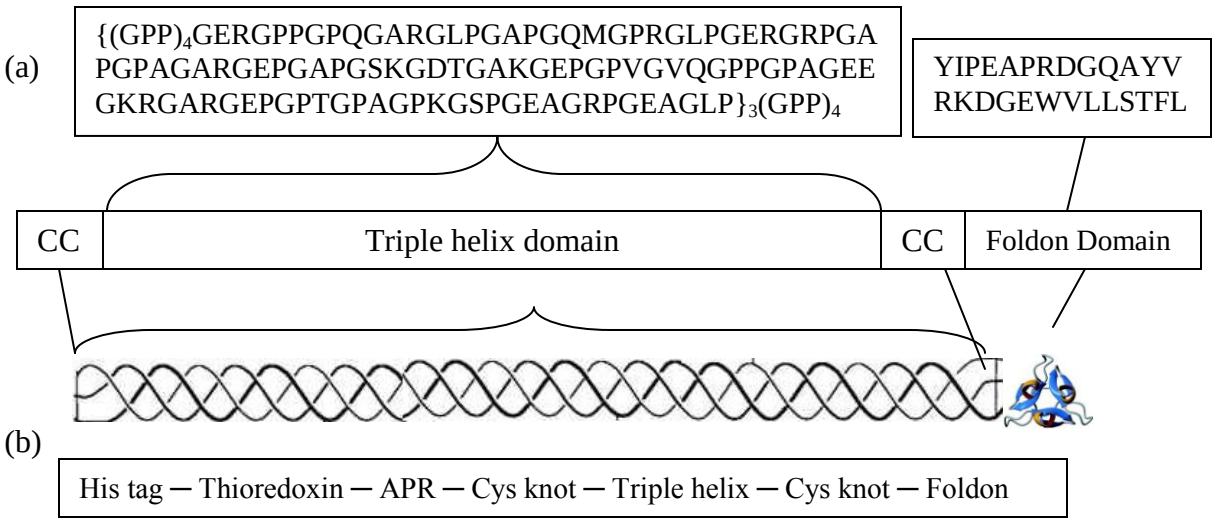

(c)

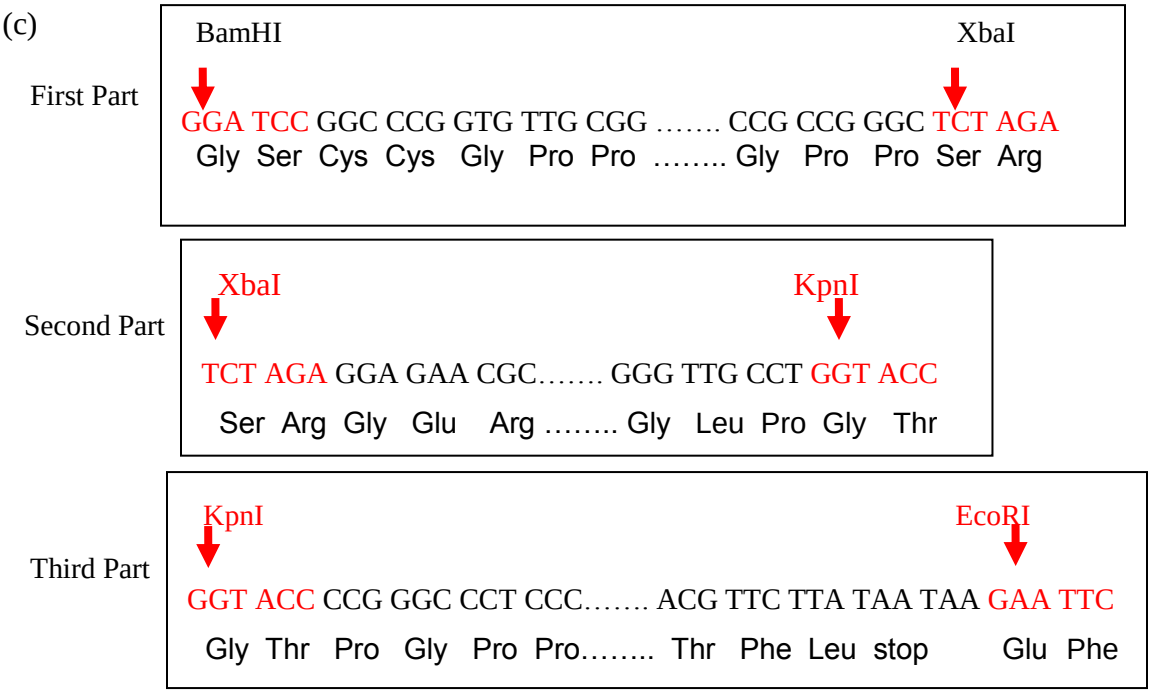
First Part
BamHI
XbaI
GGA TCC GGC CCG GTG TTG CGG ……. CCG CCG GGC TCT AGA
Gly Ser Cys Cys Gly Pro Pro …….. Gly Pro Pro Ser Arg
Second Part
XbaI
KpnI
TCT AGA GGA GAA CGC……. GGG TTG CCT GGT ACC
Ser Arg Gly Glu Arg …….. Gly Leu Pro Gly Thr
Third Part
KpnI
EcoRI
GGT ACC CCG GGC CCT CCC……. ACG TTC TTA TAA TAA GAA TTC
Gly Thr Pro Gly Pro Pro…….. Thr Phe Leu stop Glu Phe

Experiments

Synthesis of DNA sequence from three independent pieces — Since there are 411 amino acids on each monomer chain which requires 1233 bps (base pair) for DNA sequence, to reduce the risk of errors in the synthesis of entire DNA sequence, the entire DNA was divided into three pieces, and every piece owned around 400 bps and was synthesized separately, as shown in Figure 6.1(c). Then three pieces were connected each other by restriction endonuclease enzymes (5' to 3', first part and second was connected by XbaI, and second and third was KpnI) to make the complete gene. The whole 242 gene fragment was inserted to replace the section on pET32a(+) vector (Novagen Co.) bracketed between BamHI site and EcoRI site since the both ends of 242 gene had exactly identical connection sites. This pET32a(+) vector was designed for expression and purification of recombinant protein sequences. It contained inducible T7 expression region which could transcribe the coding sequences cloned by T7 RNA polymerase under control of its T7*lac* promoter, a Trx Tag thioredoxin protein (109 aa) fusing with target protein, and a cleavable His Tag for purification. Finally, the plasmid was transformed into one kind of *Escherichia Coli* (*E.Coli*) named BL21(DE3) from Novagen Co., a competent cell designed for transformation and expression of cloned fragment, and the cells were purified by ampicilin positive plates.

Expression of the Recombinant Fragments — The *E.Coli* cells including the 242 fragments were inoculated in a high-density shaking cultures, MagicMedia (Invitrogen Co.), and the 242 fusion proteins were produced by auto-induction expression through dual-temperature procedure without add-in inducer. The dual-temperature procedure is showed in the following paragraph. This MagicMedia was such a kind of culture

designed for auto-inducing the expression of target protein by the component of lactose included in the media. The entire auto-induction process was self-regulated by other components inside, which could prevent sporadic and unintended induction of expression during log-phase growth and trigger uniform and controllable induction by lactose when cultures grow to high density[208]. So the auto-inducing media could avoid addition of any inducing reagent (e.g. isopropyl-β-D-thiogalactoside, IPTG) and then avoid checking O.D. during culture growth.

Dual Temperature Procedure in MagicMedia (Invitrogen Co.) — Small inoculations of BL21(DE3) cells were done including 242 plasmids in 10 ml magicmedia overnight, shaking speed 300 rpm and temperature 37°C. As instruction of magicmedia requires, baffled flask can hold 20 % of flask volume at most and normal Erlenmeyer flask can hold 10 % of flask volume at most. 10 ml of overnight inoculation was put into 200 ml of fresh Magic Medium and place flask in shaker with speed 300 rpm and 37 ℃. The optical desorption (O.D.) of *E.Coli* culture solution that is diluted to 5% was tested and pH of *E.Coli* culture solution was test at the same time. The reason is *E.Coli* can easily grow over O.D. value of 1.0 and upper limit of UV-Vis spectrometer is 1.0 to 1.2. When O.D. of *E.Coli* reach 6.0 at around 6.5 to 7 hours, we lower down the temperature was to 25 ℃, count the starting time and leave it overnight. The whole process is called dual-temperature inducing. After 24 hours' dual-temperature auto-inducing, we transfer all medium to a 50-ml centrifuge tube and collect the cells by centrifuging with speed 2000 rpm and 4 ℃ for 20 minutes. The supernatant was removed and the cell precipitate was stored in ultralow freezer for future purification. Before collecting, we should test the

O.D. and pH again. Empirically if *E.Coli* cells made good expression, O.D. should be in the range of from 6.0 to 8.0 and pH should be around 5.0.

Basic Procedure of Isolation of 242 Protein — Since the gene product of the expressed plasmid is a fusion protein including His-tagged thioredoxin at the N-terminal end (Figure 6.1(b)), the purification of the fragments involved three steps: lysis, purification and thrombin cleavage. First we used 1 mg/ml lyzozyme solution and sonication treatment to do lysis. To prevent the protease existing in the inclusion bodies to cleavage the fusion protein, we kept adding the protease inhibitors is necessary. During the second step, the His-tagged fusion protein was purified from the cell lysate by binding with Ni-NTA metal affinity resin (Qiagen Co.) following with the purification procedure and eluted by eluting buffer containing 250 mM imidazole. To prevent precipitation forming between elution buffer and calcium ion and comply with the requirements of cleavage, we did dialysis and switch sodium dihydrogen phosphate system to Tris system before cleavage. The thrombin cleavage was carried out using Thrombin Cleave Kit (Sigma) after incubation overnight at 25 ℃. In order to test the cleavage progress, we ran SDS-PAGE (sodium dodecyl sulfate polyacrylamide gel electrophoresis) test on the after-cleavage solution that included collagen fragment and His-tagged thioredoxin fragment and the before-cleavage solution that included purified 242 fusion protein compared with the protein molecular weight marker (shown in Figure 6.2). We found the band of the His-tagged thioredoxin fragment staying at 14kDa and the band of 242 collagen monomer (the reducer in SDS gel loading buffer would dissociate triple helix trimer into three identical monomers) staying at 39 kDa, which related to the molecular weight of each fragment. Then we use HPLC to separate the His-tagged

thioredoxin fragment and the collagen fragment and lyophilize the final 242 product to dry powders. After HPLC separation, the final 242 product could have about 95% purity based on SDS-PAGE test.

Purification of 242 fusion protein by Ni-NTA resin (Qiagen Co.) — We get 6 ml of nickel agar resin solution, spin down, remove the supernatant and wash the resin by 8~10 ml wash/extract buffer. We spin down, remove the supernatant and pour the 242 lysate supernatant into the tube having resin. We seal this tube by parafilm (Fisher Sci. Co.) and put it on the shake in the big freezer and make the nickel resin bind with the His-tag of 242 fusion protein for 1 hour. The tube was centrifuged under 4 ℃ at speed of 3000 rpm for 4 minutes. The supernatant (non-binding) was transferred to a new tube and the SDS sample was prepared for the supernatant. Meanwhile we add 10 ml of wash buffer (50 mM Tris, 300 mM NaCl and 20 mM imidazole pH 8) to the resin and transfer all to the separation column (15 ml or 20 ml volume). We fix the column on a shaker and shake it for 10 min at 4 ℃. Then we fix the column on a stand, switch on the shutter and wash the resin by draining down all the liquid. We use 10~12 ml elution buffer (50 mM Tris ,300 mM NaCl and 250 mM imidazole pH 8) to wash the resin in the column and prepare 8~9 eppendorf tubes to collect the eluate results. When elution buffer is present, resin color will become darker. Normally the 1st and 2nd tubes are blank and the 3rd or 4th tube has the highest amount of 242 fusion proteins. Because the resin can be reused, we use 15 ml of 0.5 M NaOH to the column to wash for 30 min[108]. The resin can be saved in the storage buffer (30% ethanol solution)[108].

Figure 6.2 SDS-PAGE (sodium dodecyl sulfate polyacrylamide gel electrophoresis) test: fusion protein and 242 protein after Thrombin cleavage.

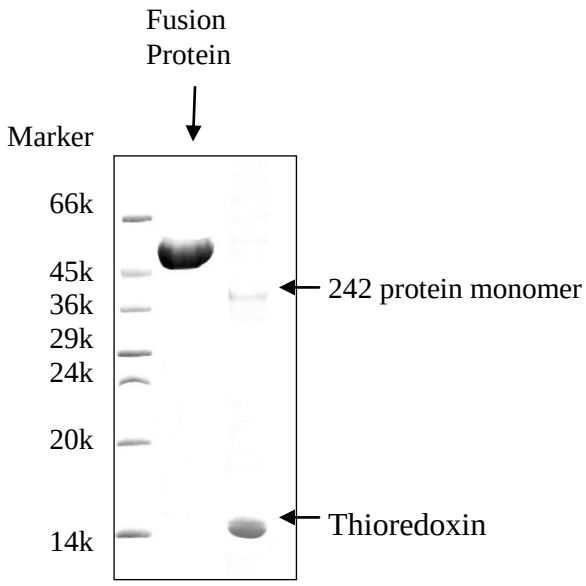

Stability testing — We did the circular dichroic (CD) spectral testing (shown in Figure 6.3(a)) and the two peaks at 225 nm (positive) and at 197 nm (negative) showed the typical peaks of collagen conformation. By testing the CD in single wavelength at 225 nm under temperature range from 4.0 °C to 65.0 °C, we got the thermal stability curve and found the melting temperature T_m of 242 protein was 39 °C from the curve (Figure 6.3(b)) which was 2 °C higher than wildtype collagen. The higher denaturation temperature means the recombinant 242 triple helix protein had higher stability than natural collagen protein and could be potentially utilized as biotemplate to nanocrystal fabrication.

Figure 6.3 (a) CD spectrum of protein 242, (b) Temperature melting curves (T_m) of the 242 collagen fragments.

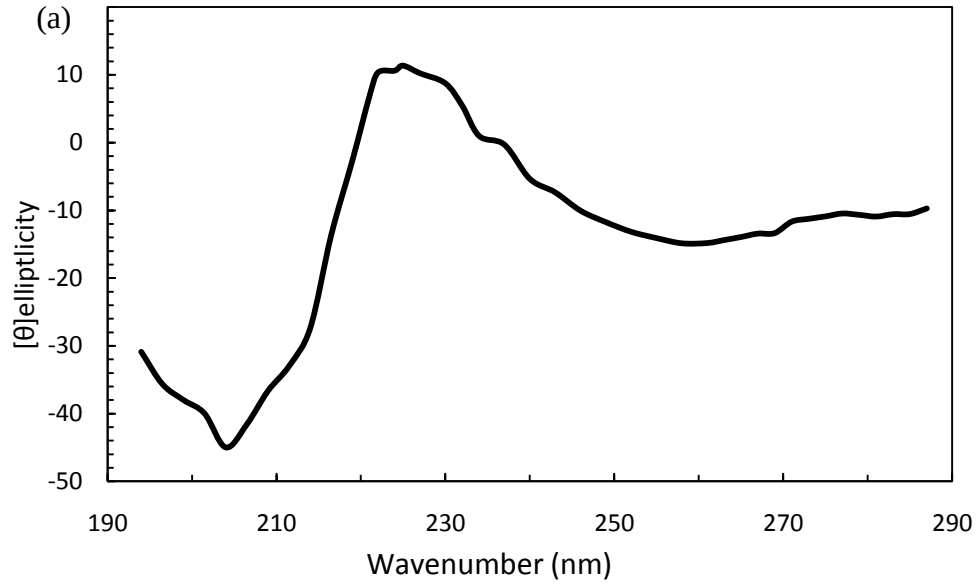

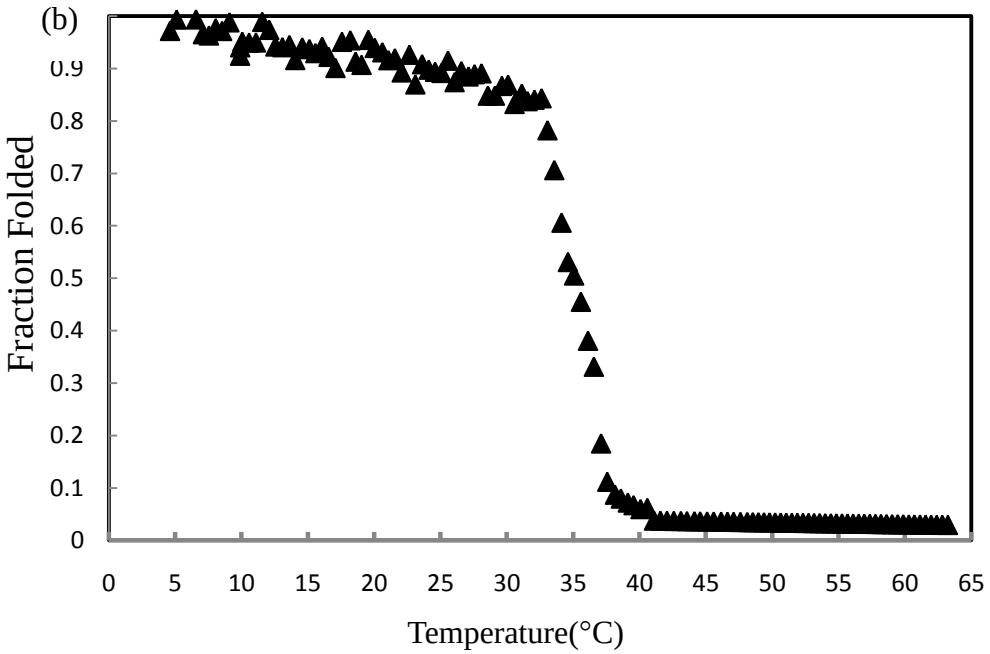

Au Nanowire Fabrication — In order to produce uniform Au coating on the biotemplate, according to the protocol in past studies, we pre-coated the triple helix with Au-mineralizing peptide, Ala-His-His-Ala-His-His-Ala-Ala-Asp (HRE, GenScript Co.), which has a high affinity for to organic Au salts [9, 115]. We mixed 40 μl of triple helix solutions (2.5 mg/ml) with 864 μl of HRE solutions (3.0×10^{-3} mg/ml) as molar ratio of 1:3 in the pH 7.0 Tris buffer solutions for one day at 4 ℃. After immobilization of HRE we added 1.3 mg of trimethylphosphinegold chloride ($AuP(CH_3)_3Cl$, Sigma Co.) as precursor into solution and made them react for four days. Then the supernatant of the solution containing unattached Au salts was removed by a pipette and 3 μl of hydrazine hydrate (Sigma) was added to reduce Au salts on triple helix complex. Meanwhile we did control experiment on neat 242 triple helix protein without HRE peptide to make reaction with Au precursor, that was same amount of triple helix solution mixing with the same buffer solution as in HRE solution reacting with same precursor under exactly same reaction conditions and time length. All the samples including 242 protein, complex of HRE and 242 protein, Au-coated HRE-242 result and Au-coated 242 result were tested with transmission electron microscope (TEM) in dry state. The protein samples were first negative stained by 2%wt of uranyl acetate staining reagent and then prepared on the carbon-formvar-film copper TEM grids dried by filter paper piece. And the Au-coat samples were prepared on the carbon-film nickel TEM grids and dried too. The images were taken by Zeiss EM 902 TEM at an acceleration voltage of 80 kV and electron diffractions were gotten at JOEL 1200 EX TEM at an acceleration voltage of 100 kV. All results were similar to the past study on F877 triple helix protein, which meant the 242

triple helix protein was able to apply as biotemplate as F877 for the fabrication of metal crystal nanowires.

Figure 6.4. TEM images of the 242 triple helix peptides (a) in neat, (b) coated by Au, (c) coated by HRE-mineralizing peptides. (d) TEM image of the HRE-coated triple helix peptides (c) coated by Au. Electron diffraction patterns of (b) and (d) are shown next to their TEM images. The size distribution of Au nanowires is shown in (e).

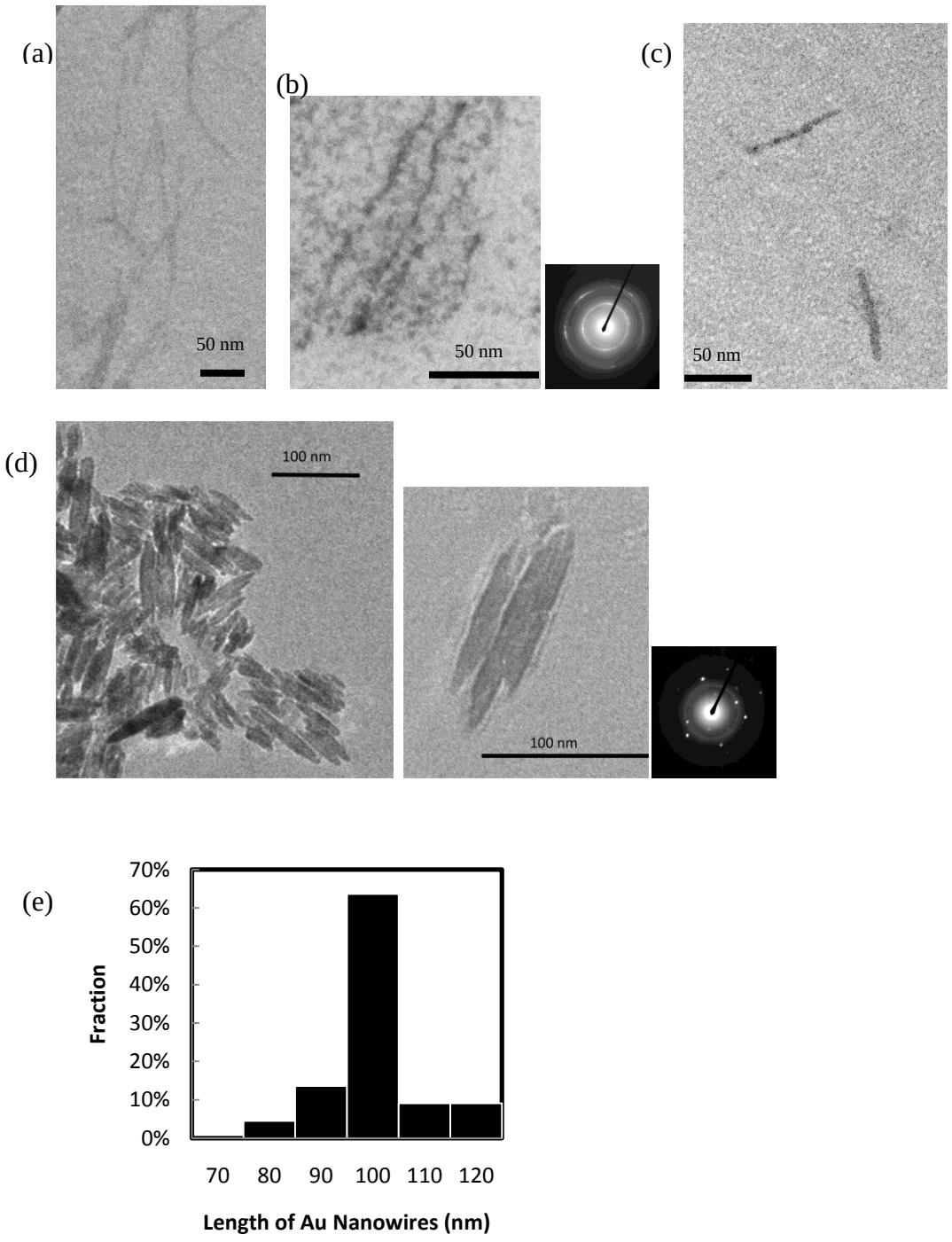

Results and Discussions

From the TEM result of Figure 6.4(a), the 242 triple helix protein molecule formed nanowires having uniform size of 100 nm × 4 nm, which indicated a rigid conformation. The length was consistent with the value of the 98 nm end-to-end distance of a single triple helix consisting of 372 amino acids and a foldon domain estimated from the crystal structure of the triple helix[206]. The observed diameter of 4 nm appeared to be larger than the 1-2 nm predicted from the crystal structure. This slightly larger diameter in TEM image could be caused by swelling via hydration[209]. Comparing with the size value 40 nm × 4 nm of F877 triple helix protein[9], we could conclude the artificial triple helix proteins have monodispersed size that were determined only by the amino acid sequence on the triple helix domain and could be easily varied or customized by modifying the recombinants.

To test the feasibility of 242 triple helix protein biotemplate, after the protein solution was incubated with Au precursor trimethylphosphinegold chloride for four days and then with reducing reagent hydrazine hydrate for one day both at 4 ℃, Au crystals were grown on the protein. As shown in Figure 6.4(b), the TEM image showed that the Au nanocrystal growth was localized on the protein molecule surface, the Au coating was incontinuous on the entire protein template and the size of Au nanocrystals were not well controlled.

In order to make uniform and continuous Au nanocrystal growth, we introduced the Au-metal-affinity-and-mineralizing peptide HRE to pre-coat onto the 242 triple helix surface to form complex through hydrogen bondings. As the TEM image shown in Figure 6.4(c), no significant changes in length, diameter, and shape were detected after the triple

helix was coated by HRE. The subsequent Au electroless process on these HRE-bound complex yielded uniform Au nanowires. The reduction of Au on the HRE-coated triple helix produced uniform and highly crystalline Au coating on the surface with defined dimension of 100 nm × 10 nm, the TEM images and diffraction were shown in Figure 6.4(d) and inset, and the size distribution of Au nanowires was shown in Figure 6.4(e). The Au-coated triple helix in the inset of Figure 6.4(d) appears to be a shuttle-like oval shape, which could be due to the inhomogeneous coating of HRE peptide at the ends[9]. The foldon at C-terminal end formed a three stranded β-hairpin propeller[206], a conformation very different from that of the triple helix, and the conformation differences resulted in the different bindings of the HRE peptides and less Au growth on those areas as compared to the middle part of triple helix, consistent with the shuttle-shape formation. We observed the similar behaviors happened in Au nanocrystal growing on F877-HRE complex in the past studies. From these studies, we could conclude that the artificial collagen-like triple helix was a reliable biotemplate to make monodispersed size nanofabrications and the protocol of pre-coating certain metal-affinity-and-mineralizing peptide was an approved strategy to make uniform crystal growth.

Conclusion

In summary, an artificial collagen-like triple helix was designed by recombinant technology and successfully synthesized from *E. coli* expression system. Similar as the strategy on the design F877 triple helix protein, the fragments that have high thermal stability from natural collagen I chain were selected onto the 242 triple helix protein

sequence to make homo trimer of triple helix backbone and the stability-intensify sequences such as Cysteine knot and foldon were successfully used on this triple helix sequence to strengthen the stability of entire biomolecule of 242 protein. Compared with previous F877 triple helix protein, this new 242 protein had bigger size in length and was able to be more widely used for making bigger metal nanowires as biotemplates since the size of 242 protein was easier to be detected by other instruments such as atomic force microscopy (AFM) and to build complex bioconstructions. Same as F877 case on nanowire fabrication, the length of the nanowires made on 242 template can be easily controlled by the number of amino acid residues, and the production of protein can be scaled up by means of the cell multiplication. The successful trials on the F877 and 242 triple helix proteins proved a practical way to obtain and customize diverse size nanowires based on the biotemplate of collagen-like triple helix proteins combined with the versatility of the recombinant technology.

Chapter 7. Doughnut-Shaped C7 Peptide Nano-Assemblies and Their Applications as Nanoreactors to make Size-Controlled Silica Nanoparticles

Introduction

Nanomaterial synthesis is emerging as a crucial branch in nanotechnology to develop building blocks for nanometerscale devices. To synthesize nanomaterials in controlled sizes and dimensions, various types of nanoreactors, nanometer-sized chemical reaction vessels, have been developed[210-216]. The nanoreactors are applied not only in material syntheses but also in controlled release and drug delivery. One advantage of nanoreactor is to manipulate the size of the nanoparticles. Controlling sizes of nanoparticles is becoming apparently important in various practical applications since chemical and physical properties of nanoparticles can be tunable by their sizes and shapes[217, 218]. For example, different sizes of nanoparticles have different absorption properties so that the size control can create a new set of colors of the nanoparticles[219].

There is a method to control the size of nanoparticles by nanoreactors. We focused on the ring-shaped or doughnut-shaped nanoreactors because those ones introduce well-defined growth areas within cavities, which offer straightforward size control of nanomaterials[220, 221]. Micelles and polyelectrolytes have convenient and flexible cavities that function as nanoreactors[211, 222-224], but more stable assemblies against broad ranges of precursors and chemical reagents are desirable to synthesize a variety of nanomaterials. Here we introduce a doughnut-shaped nanoreactor, C7 peptide nano-doughnuts. The nano-doughnuts were self-assembled from C7 peptides (molecular structure shown in Scheme 7.1(a)) and metal or semiconductor precursor. The previous five years, there were reports about various shapes of peptide/protein assemblies produced in

biomaterials[113, 203, 225-229]. The past study of our lab demonstrated that monodispersed metal nanocrystals such as gold or semiconductor nanocrystals such as barium titanate were grown inside the cavities of peptide nanodoughnuts via trapping precursor ions into the cavities at room temperature. The consequent Au nanocrystals were extracted by destroying the nano-doughnuts via long UV irradiation[220]. The cavities of doughtnut-shaped reactors bound the barium titanate precursors via chelation by carbonyl groups of the C7 peptide, catalyzed the hydrolysis and condensation/polymerization process by their own special local reacting environment[230] and finally barium titanate nanoparticles were achieved[221].

Now we made another trial to fabricate silica (SiO_2) nanoparticles by using this doughnut-shaped nanoreactor in a biomimetic process like biosilicification taking place in natural marine organisms[230-232]. Silicon (Si) is the second most abundant element on Earth and is widely used in the manufacture of numerous siloxane-based materials,including semiconductors, glasses, ceramics, plastics, elastomers, resins, mesoporous molecular sieves and catalysts, and optical fibers and coatings[233, 234]. The manufacturing of these materials typically requires high temperatures and pressures or the use of caustic chemicals. In contrast, the biological production of silica is accomplished under mild physiological conditions and produces remarkably exquisite structures. Thousands of living species produce ordered silica structures under mild physiological conditions of near-neutral pH and low temperature. The biological syntheses of silica demonstrate that these species have evolved novel mechanisms for the control of siloxane polycondensation[230]. Amino acids play an important role for the catalytic activity of enzyme or protein to the hydrolysis of alkyloxysilane precursors such

as serine and histine on silicatein enzyme for biosilicification. Since silicatein is a structurally and functionally related enzyme, the alcohol side chain of serine at position 26 and imidazole side chain of imidazole at position 165 are critical for the effectiveness of the catalytic sites on silicatein[235]. There was a study that mimicked the catalysis function with small organic molecules such as ethonalamine which had similar nucleophilic function group as serine at position 26 on silicatein, the process proceeded at neutral pH, room temperature and the results indicated ethonalamine had a modest catalytic effect on the hydrolysis and polymerization of silicon ethoxides compared with other small organic molecules[230]. As a result, amorphous and polydispersed silica products were obtained. Inspired by the past study, we assume the amine group and hydroxyl group of C7 peptide can perform the similar catalysis on the hydrolysis of alkyloxysilane precursors because ethonalamine molecule also has both function groups. Hence we can design a similar experiment under the same conditions (neutral pH, room temperature and same silicon ethoxide precursor).

Scheme 7.1 (a) Illustration of the peptide structure, (b)the self-assemble of the peptide to form nano-doughnut reactor to chelate precursor, (c) SiO_2 nanoparticle form inside the cavity of nano-reactor after hydrolysis and condensation.

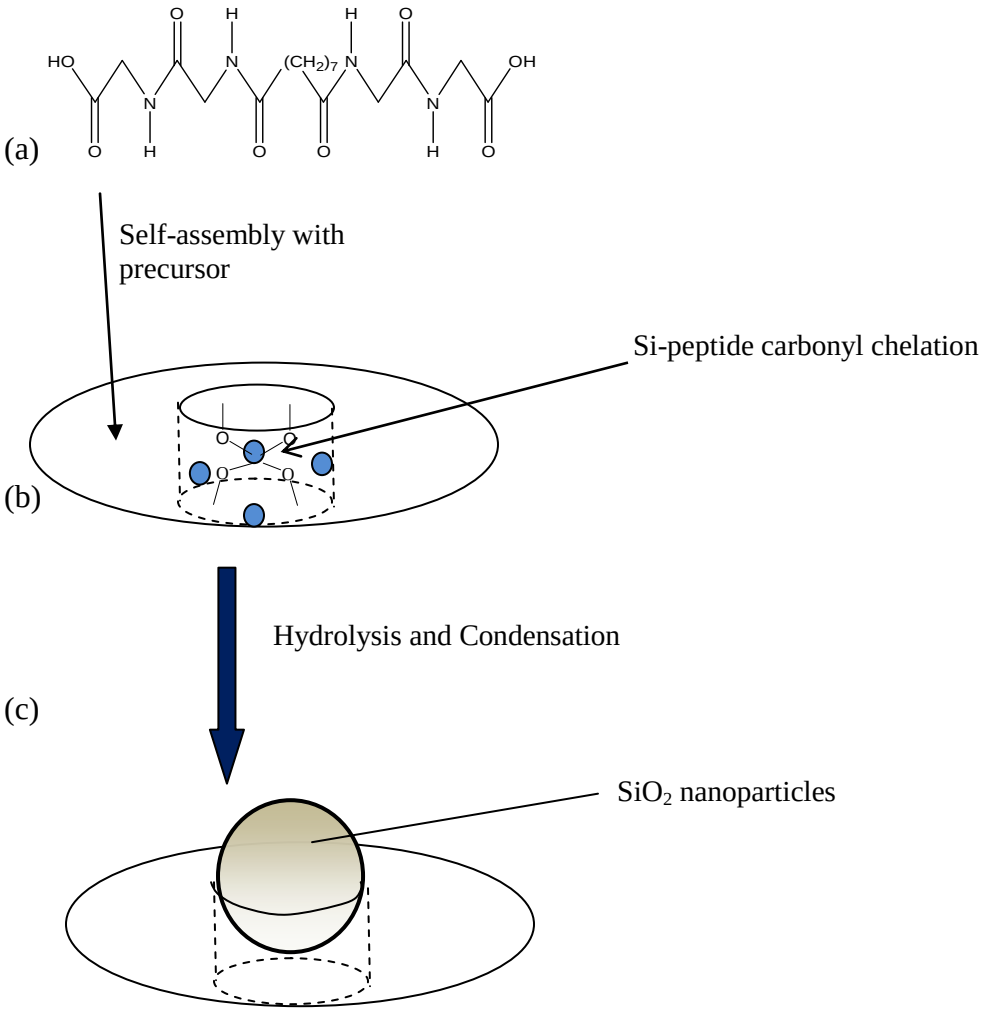

Experiments

The C7 glycylglycine bolaamphiphilic peptide was synthesized in our lab by the organic synthesis method. First we made the reaction of connecting EDAC activated Gly-Gly-Benzyl-Ester (Sigma Co.) with both ends of azelaic acid (Sigma Co.) in dimethylformalmide (DMF) solvent, and the entire reactor was kept in ice bath. Second we evaporate out the solvent by rotovaping and filter out impurities. Third we do recrystallization on intermediate to further remove impurities, then redissolve the intermediate in DMF and do base-hydrolysis for four hours under 75~85 ℃. Last we do rotovap again and obtain final C7 monomer product in white color[236-238].

The Si precursor was tetraethoxysilane (TEOS, $Si(OEt)_4$, Acros Co.) according to the literature about mimic test by small molecule ethanolamine[230]. First we dissolved 0.0208g of C7 monomer powder (0.005 mol) in 6.6 ml H_2O and 3.3 ml NaOH, used syringe filter to remove insoluble stuff, then adjusted pH to different values (4.5, 7.0 and 10.0) by 0.1 mol/l citric acid. Second we added 10 μl of TEOS to the C7 peptide solution, (because vapors of TEOS could cause blindness, operation had to do in fume hood), covered the reacting container with aluminum foil paper (Fisher Sci. Co.) because C7 peptide would decompose under UV light. After incubation for one day and three days, we pick up 10 μl of solution to prepare TEM samples and AFM (atomic force microscopy) samples. As literature illustrated, we expect to see monodispersed silica nanoparticles in neutral condition. The TEM sample was prepared by dropping solutions onto carbon-coated copper TEM grids and drying the excess solution by filter papers. The dried TEM grids were then examined for imaging and the electron diffraction pattern with a JOEL 1200 EX TEM at an acceleration voltage of 100 kV. The AFM sample was

prepared by dropping solution onto round mica slice attached on a round iron substrate, spreading the liquid by spinning it on battery-powered motor plate and then drying in the air. The AFM was test and images were acquired with a Nanoscope III (Vecco, Inc.) AFM. Meanwhile Raman spectra of pure C7 peptide and dried silica results were tested on a confocal Raman microscope (LabRam, JobinYvon/Horiba). The 632.8 nm line of an air-cooled He/Ne laser was injected into an integrated Olympus BX 40 microscope and focused to a spot size of approximately 0.7 μm by an 80 fold long-working-distance objective.

Figure 7.1 TEM images of silica nanoparticles surrounded by C7 peptide self-assemble nanodought-shaped reactor after C7 peptide reacting with TEOS (a) at pH 7.0, one day reaction, followed with electron diffraction (ED) pattern; (b) at pH 7.0, three days, inset was the HRTEM of single particle (scale bar 100 nm), followed with ED, (c) at pH 4.5, one day, followed with ED. Scale bar : 200 nm.

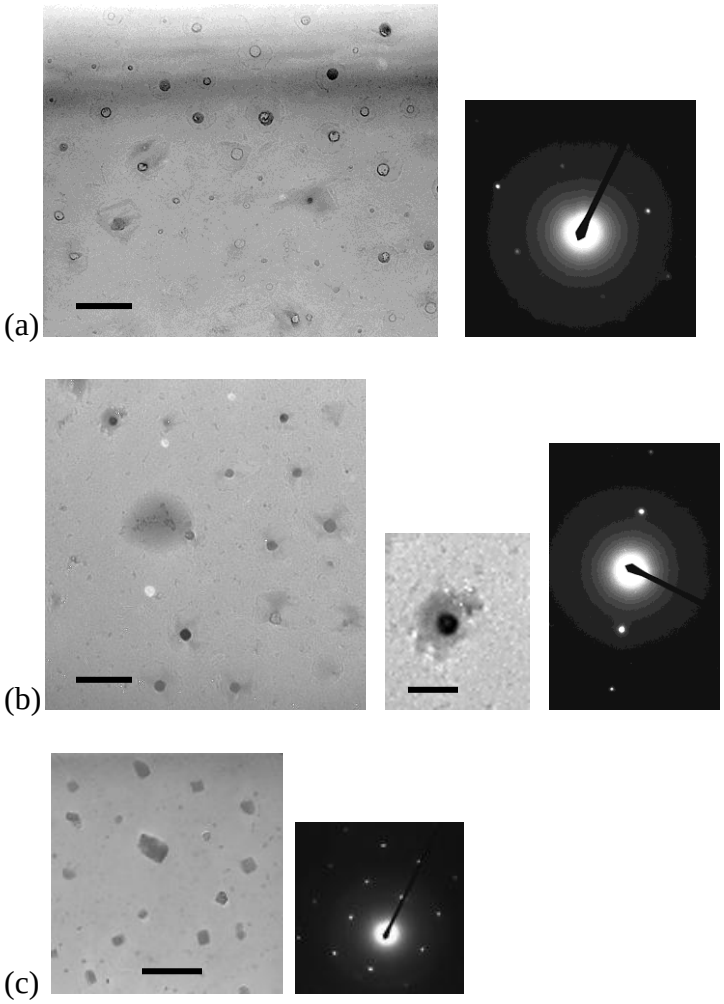

Results and Discussions

As we predicted based on the references [230, 233, 239], the uniform silica (SiO_2) nanoparticles appeared only at neutral pH condition. In acid condition (pH 4.5) shown in Figure 7.1(c), the silica nanocrystals also showed up but the size was polydispersed and shape were various. From the electron diffraction pattern of Figure 7.1(c), the crystal structure was cubic type; however after we calculated the crystal structural parameters, the result did not match any current silica crystal category. On the contrary, in basic condition (pH 10.0), amorphous silica particles were acquired which suggested the hydrolysis reaction was more vigorous than other two conditions and was uncontrollable. Only in neutral pH condition, both chelation and hydrolysis process were under control. First only in this condition, the self-assembled doughnut-shaped reactors formed via hydrogen bonds between carboxylic groups and amine groups from C7 peptides [221, 240], at the same time, the carbonyl groups chelated and fixed the Si precursor. Then the rest hydroxyl groups and the rest amine groups in the cavity region performed their catalysis function for the hydrolysis and condensation of SiO_2 like the same kind of effects from ethanolamine molecules. We presumed SiO_2 nanocrystals started to grow at the place inside the cavity of doughnut-shaped reactor, and then more crystals would continue growing in the direction pointing to the center of the cavity as time goes by until the whole cavity is filled. The TEM images of one day reaction and three days reaction confirmed our assumption. In Figure 7.1(a), doughnut-shaped nanoreactors formed and SiO_2 crystals appeared at the place tightly close to the inside ring of cavity. One day reaction time was not enough for SiO_2 crystal accumulation to fill the whole cavity and we observed ring-shaped SiO_2 nanocrystal. After three days' growth and accumulation,

as shown in Figure 7.1(b), most cavities were filled with SiO_2 crystals and uniform size nanoparticles were achieved that could be readily harvested by irradiating UV light to decompose C7 peptide doughnut-shaped reactors[220, 221]. After calculated the parameters of ED pattern, we found the crystal structure matched the cristobalite crystal category for SiO_2. As we know, the formation of cristobalite crystals normally took place in high temperature and high pressure condition. So the successful achievement of cristobalite crystal at room temperature illustrated a novel way to synthesize this kind of hard and rigid crystal structure which required much less energy consumption and carried on more economically compared with classical ways. This biomimetic result was consistent with the unusual silica crystal structures forming in biosilification process taking place in natural organism.

From the phase channel image of AFM in Figure 7.2(a), we could observe another picture of the results where nano doughnut-shaped reactor surrounding the silica particles in terms of height. The silica core is much higher than C7 peptide doughnut shell thus the center cores showed higher height value than the doughnuts surrounding them. Due to the limitation of AFM tip, we could not see the ring shape crystal accumulation at centers of all doughnuts.

From the Raman spectra shown in Figure 7.2(b), there were discrepancies of peaks between the pure C7 peptide and silica doughnut product in the region from 1600 to 1700 cm^{-1}, and this region called as Amide I region represent the C=O stretches in amide groups. Raman spectra indicated that the two peaks at 1638 $cm^{-1}$and 1660 cm^{-1} existing in C7 peptide disappeared while silica precursor reacted with peptide, which could be explained that the carbonyl group attended the chelating with precursor and then the

stretch peaks were weakened by chelation. On the other hand, Raman spectral discrepancies confirmed the trapping and fixing effects of the carbonate groups in the region of cavity.

Since the C7 glycylglycine bolaamphiphilic peptides is capable to self-assemble to doughnut-shaped nanoreactors with precursor and catalyze the hydrolysis by chelating, after this successful trial on silica, we have assayed the precursors for other element, such as titanium and aluminum, to make size-controlled nanoparticle. Similar to the strategy as TEOS, where we picked up an alkyloxy salt as a precursor, we utilized titanium isopropoxide ($Ti(O–isoPro)_4$) , aluminum isopropoxide ($Al(O–isoPro)_3$) and aluminum butyroxide ($Al(O–(CH_2)_3CH_3)_3$) to react with C7 monomer solution under same conditions. Results were disappointing, poly-dispersed particles were obtained and more aggregates could be observed everywhere on TEM sample grid. We think the hydrolysis of these precursors could be too strong to control by C7 peptide or the precursors we selected which were not the suitable ones. Nonetheless, these trials were the reference for future study to avoid failure experience.

Figure 7.2 (a) AFM image of silica nanoparticles surrounded by C7 peptide self-assemble nanodought-shaped reactor in neutral condition, reacting time: one day. Scale bar 100 nm, height channel image. (b) Raman spectrum of pure C7 peptide (up) and C7 peptide reacting with Si precursor (down), two assigned peaks in Amide I region were indicated by arrows.

(a)

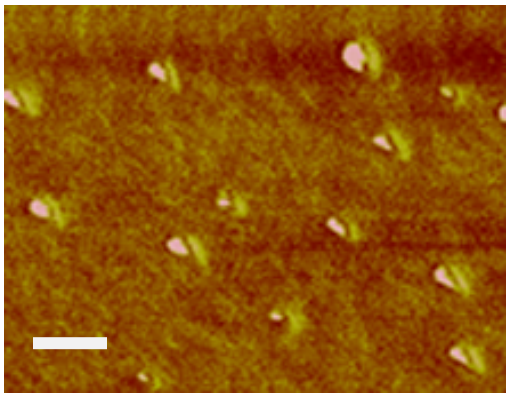

(b)

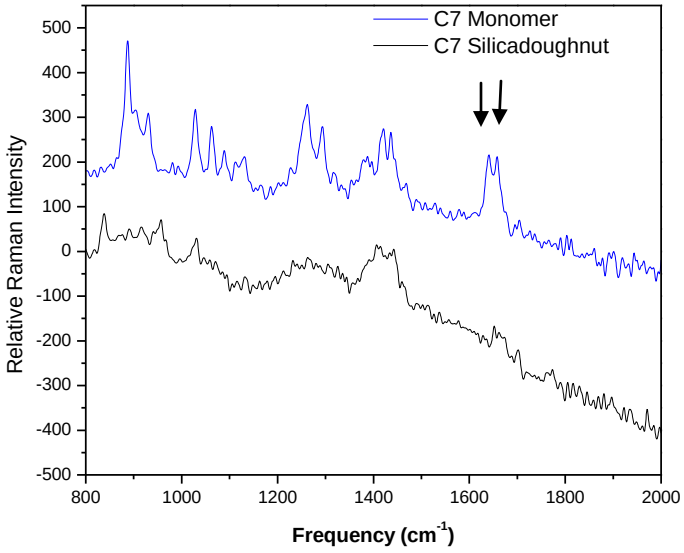

Conclusion

In summary, room temperature synthesis of silica nanocrystal with certain crystal category were achieved under neutral pH condition and monodispersed silica nanoparticles were harvested via the controlling of C7 peptide self-assembled doughnut-shaped nanoreactors. The hydroxyl groups and the amine groups from glycylglycine bolaamphiphiles would interfere with the hydrolysis of silica precursors under those conditions above, which were consistent with the previous study of small molecules owing same function groups.

References

1. G. M. Malacinski and D. Freifelder, *Essentials of Molecular Biology*, Jones and Bartlett Publishers, Boston, 1998.
2. K. E. KADLER, D. F. HOLMES, J. A. TROTTER and J. A. CHAPMAN, *Biochem. J.*, 1996, **316**, 1.
3. H. Bai, K. Xu, Y. Xu and H. Matsui, *Angew. Chem. Intl. Ed.*, 2007, **46**, 3319-3322.
4. H. Bai, F. Xu, L. Anjia and H. Matsui, *Soft Matter*, 2009, **5**, 966.
5. K. Xu, I. Nowak, M. Kirchner and Y. Xu, *J. Biol. Chem.*, 2008, **283**, 34337.
6. S. R. Whaley, D. S. English, E. L. Hu, P. F. Barbara and A. M. Belcher, *Nature*, 2000, **405**, 665.
7. E. Braun, Y. Eichen, U. Sivan and G. Ben-Yoseph, *Nature*, 1998, **391**, 775.
8. X. Gao and H. Matsui, *Adv. Mater.*, 2005, **17**, 2037-2050.
9. H. Bai, K. Xu, Y. Xu and H. Matsui, *Angew. Chem. Int. Ed.*, 2007, **46**, 3319.
10. S. W. Chung, D. S. Ginger, M. W. Morales, Z. F. Zhang, V.Chandrasekhar, M. A. Ratner and C. A. Mirkin, *Small*, 2005, **1**, 64.
11. I. A. Banerjee, L. Yu and H. Matsui, *J. Am. Chem. Soc.*, 2005, **127**, 16002.
12. Z. Deng, Y. Tian, S. H. Lee, A. E. Ribbe and C. D. Mao, *Angew. Chem. Int. Ed.* , 2005, **44**, 3582.
13. R. Djalali, Y.-F. Chen and H. Matsui, *J. Am. Chem. Soc.*, 2003, **125**, 5873.
14. C. B. Mao, D. J. Solis, B. D. Reiss, S. T. Kottmann, R. Y. Sweeney, A. Hayhurst, G. Georgiou, B. Iverson and A. M. Belcher, *Science*, 2004, **303**, 213.
15. M. Reches and E. Gazit, *Science*, 2003, **300**, 62.

16. J. Sharma, R. Chhabra, Y. Liu, Y. G. Ke and H. Yan, *Angew. Chem.Int. Ed.*, 2006, **45**, 730.

17. J. Richter, *Physica E*, 2003, **16**, 157.

18. F. Patolsky, Y. Weizmann and I. Willner, *Nat.Mater.*, 2004, **3**, 692.

19. M. Reches and E. Gazit, *Science*, 2003, **300**, 625.

20. T. Scheibel, R. Parthasarathy, G. Sawicki, X. M. Lin, H. Jaeger and S. L. Lindquist, *Proc. Natl. Acad. Sci., U.S.A.*, 2003, **100**, 4527.

21. A. J. Patil, E. Muthusamy, A. M. Seddon and S. Mann, *Adv.Mater.*, 2003, **15**, 1816.

22. S. A. Davis, S. L. Burkett, N. H. Mendelson and S. Mann, *Nature*, 1997, **385**, 420.

23. C. Li and J. H. He, *Langmuir*, 2006, **22**, 2827.

24. E. Royston, S. Lee, J. N. Culver and M. T. Harris, *J.Colloid Interface Sci.*, 2006, **298**, 706.

25. Z. Li, S. Chung, J. M. Nam, D. S. Ginger and C. A. Mirkin, *Angew. Chem. Int. Ed.*, 2003, **42**, 2306.

26. N. NURAJE, K. SU, J. SAMSON, A. HABOOSHEH, R. I. MACCUSPIE and H. MATSUI, *Supramolecular Chemistry*, 2006, **18**.

27. M. Endo, H. X. Wang, M. Fujitsuka and T. Majima, *Chem. Eur. J.*, 2006, **12**, 3735.

28. H. M. Yi, S. Nisar, S. Y. Lee, M. A. Powers, W. E. Bentley, G. F.Payne, G. W. Rubloff, M. T. Harris and J. N. Culver, *Nano Lett.* , 2005, **5**, 1931.

29. R. J. TSENG, C. TSAI, L. MA, J. OUYANG, C. S. OZKAN and Y. YANG, *Nature*, 2006, **1**, 72.

30. A. Rich and F. H. C. Crick, *J. Mol. Biol.* , 1961, **3**, 483.

31. T. A. Shannon, *Genetic Engineering*, Greenwood Press, London, 1999.

32. J. D. Watson, R. M. Myers, A. A. Caudy and J. A. Witkowski, Cold Spring Harbor Lab Press, New York, 2007, p. 474.

33. B. BRODSKY and A. V. PERSIKOV, *Advances in Protein Chemistry*, 2005, **70**, 301.

34. J.Bella, M.Eaton, B.Brodsky and H.M.Berman, *Science*, 1994, **266**.

35. C. G. Knight, L. F. Morton, A. R. Peachey, D. S. Tuckwell, R. W. Farndale and M. J. Barnes, *J. Biol. Chem.*, 2000, **275**, 35.

36. C. M. Kielty and M. E. Grant, in *Connective Tissue and its Heritable Disorders*, eds. P.M.Royce and B. Steinmann, Wiley-Liss, New York, 2002, p. 159.

37. C. L. Jenkins and R. T. Raines, *Nat. Prod. Rep.*, 2002, **19**, 49.

38. D. J. Hulmes, *J. Struct. Biol.*, 2002, **137**, 2.

39. S. Perumal, O. Antipova and J. P. Orgel, *Proc Natl Acad Sci*, 2008, **105**, 2824.

40. R. Z. Kramer, J. Bella, B. Brodsky and H. M. Berman, *J. Mol. Biol.*, 2001, **311**, 131.

41. A. V. Persikov, J. A. Ramshaw, A. Kirkpatrick and B. Brodsky, *Biochemistry*, 2000, **39**, 14960.

42. G. A. D. LulloDagger, S. M. Sweeney, J. Körkkö, L. Ala-Kokko and J. D. S. Antonio, *J. Biol. Chem.*, 2002, **277**, 4223.

43. G. N. Ramachandran and G. Kartha, *Nature*, 1954, **174**, 269.

44. G. N. Ramachandran and G. Kartha, *Nature*, 1955, **176**, 593.

45. T. J. Wess, *J Mol Biol*, 1998, **275**, 255.

46. R. Z. Kramer, M. G. Venugopal, J. Bella, P. Mayville, B. Brodsky and H. M. Berman, *J. Mol. Biol.*, 2000, **301**, 1191.

47. H. P. Bachinger, P. Bruckner, R. Timpl, D. J. Prockop and J. Engel, *Eur. J. Biochem.* , 1980, **106**, 619.

48. T. Koide, *Connective Tissue Research*, 2005, **46**, 131.

49. S. Boudko, S. Frank, Kammerer R.A., S. J., S. T., L. R., L. A., B. H.P. and J. Engel, *J. Mol. Biol.*, 2002, **317**, 459.

50. J. P. Orgel, *Proc Natl Acad Sci*, 2006, **103**, 9001.

51. R. D. B. Fraser, T. P. MacRae, A. Miller and E. Suzuki, *J. Mol. Biol.* , 1983, **167**, 497.

52. R. D. Fraser, T. P. MacRae and A. Miller, *J Mol Biol*, 1987, **193**, 115.

53. T. Koide and K. Nagata, *Top Curr. Chem.*, 2005, **247**, 85.

54. K. Okuyama, S. Arnott, M. Takayanagi and M. Kakudo, *J. Mol. Biol.*, 1981, **152**, 427.

55. J. Engel and H. P. Bächinger, *Top Curr. Chem.*, 2005, **247**, 7.

56. K. Beck and B. Brodsky, *J. Struct. Biol.* , 1998, **122**, 17.

57. D. E. Birk and P. Bruckner, *Top Curr. Chem.*, 2005, **247**, 185.

58. G. Ramachandran, *Structure of collagen at the molecular level*, Academic Press, New York, 1967.

59. G. N. Ramachandran and R. Chandrasekharan, *Biopolymers*, 1968, **6**, 1649.

60. E. Suzuki, R. D. B. Fraser and T. P. MacRae, *Int. J. Biol. Macromol.*, 1980, **2**, 54.

61. P. L. Privalov, *Adv. Prot. Chem.*, 1982, **35**, 1.

62. Y. Xu, T. Hyde, X. Wang, M. Bhate and B. Brodsky, *Biochemistry*, 2003, **42**, 8696.

63. J. Bella and H. M. Berman, *J. Mol. Biol.*, 1996, **264**, 734.

64. W. Traub and K. A. Piez, *Adv. Prot. Chem.*, 1971, **25**, 243.

65. S. Leikin, V. A. Parsegian, W.-H. Yang and G. E. Walrafen, *Proc. Natl. Acad. Sci.*, 1997, **94**, 11312.

66. S. Leikin, D. C. Rau and V. A. Parsegian, *Proc. Natl. Acad. Sci.* , 1994, **91**, 276.

67. S. Leikin, D. C. Rau and V. A. Parsegian, *Nat. Struct. Biol.* , 1995, **2**, 205.

68. J. Stetefeld, S. Frank, M. Jenny, T. Schulthess, R. A. Kammerer, S. Boudko, R. Landwehr, K. Okuyama and J. Engel, *Structure*, 2003, **11**, 339.

69. P. Bruckner, E. F. Eikenberry and D. J. Prockop, *Eur. J. Biochem.*, 1981, **118**, 607.

70. H. P. Bachinger, P. Bruckner, R. Timpl and J. Engel, *Eur. J. Biochem.* , 1978, **90**, 605.

71. H. P. Bachinger and J. M. Davis, *Int. J. Biol. Macromol.*, 1991, **13**, 152.

72. A. V. Persikov, J. A. M. Ramshaw, A. Kirkpatrick and B. Brodsky, *Biochemistry*, 2005, **44**, 1414.

73. A. V. Persikov, J. A. M. Ramshaw and B. Brodsky, *J. Biol. Chem.*, 2005, **280**, 19343.

74. J. G. Bann and H. P. Bachinger, *J. Biol. Chem.*, 2000, **275**, 24466.

75. S. Meier, S. Güthe, T. Kiefhaber and S. Grzesiek, *J. Mol. Biol.*, 2004, **344**, 1051.

76. S. Güthe, L. Kapinos, A. Möglich, S. Meier, S. Grzesiek and T. Kiefhaber, *J. Mol. Biol.*, 2004, **337**, 905.

77. D. E. Mechling and H. P. Bächinger, *J. Mol. Biol.*, 2000, **275**, 14532.

78. Y. Tao, S. V. Strelkov, V. V. Mesyanzhinov and M. G. Rossmann, *Structure*, 1997, **5**, 789.

79. S. R. Whaley, D. S. English, E. L. Hu, P. F. Barbara and A. M. Belcher, *Nature*, 2000, **405**, 665-668.

80. E. Braun, Y. Eichen, U. Sivan and G. Ben-Yoseph, *Nature*, 1998, **391**, 775.

81. J. Sharma, R. Chhabra, Y. Liu, Y. G. Ke and H. Yan, *Angew. Chem. Int. Ed.*, 2006, **45**, 730-735.

82. Z. X. Deng, Y. Tian, S. H. Lee, A. E. Ribbe and C. D. Mao, *Angew. Chem. Int. Ed.*, 2005, **44**, 3582-3585.

83. M. Reches and E. Gazit, *Science*, 2003, **300**, 625-627.

84. M. G. Ryadnov and D. N. Woolfson, *J. Am. Chem. Soc.*, 2004, **126**, 7454-7455.

85. K. Sugimoto, S. Kanamaru, K. Iwasaki, F. Arisaka and I. Yamashita, *Angew. Chem. Int. Ed.*, 2006, **45**, 2725-2728.

86. W. Shenton, T. Douglas, M. Young, G. Stubbs and S. Mann, *Adv. Mater.*, 1999, **11**, 253.

87. R. J. Tseng, C. Tsai, L. Ma, J. Ouyoung, C. S. Ozkan and Y. Yang, *Nature Nanotech.*, 2006, **1**, 72-77.

88. S. W. Chung, D. S. Ginger, M. W. Morales, Z. F. Zhang, V. Chandrasekhar, M. A. Ratner and C. A. Mirkin, *Small*, 2005, **1**, 64-69.

89. S. Behrens, J. Wu, W. Habicht and E. Unger, *Chem. Mater.*, 2003, **16**, 3085-3090.

90. M. Knez, M. Sumser, A. M. Bittner, C. Wege, H. Jeske, T. P. Martin and K. Kern, *Adv. Func. Mater.*, 2004, **14**, 116-124.

91. R. Djalali, Y.-F. Chen and H. Matsui, *J. Am. Chem. Soc.*, 2003, **125**, 5873-5879.

92. I. A. Banerjee, L. Yu and H. Matsui, *J. Am. Chem. Soc.*, 2005, **127**, 16002-16003.

93. C. B. Mao, D. J. Solis, B. D. Reiss, S. T. Kottmann, R. Y. Sweeney, A. Hayhurst, G. Georgiou, B. Iverson and A. M. Belcher, *Science*, 2004, **303**, 213-217.

94. I. A. Banerjee, L. Yu and H. Matsui, *Proc. Natl. Acad. Sci. USA*, 2003, **100**, 14678-14682.

95. L. Yu, I. A. Banerjee, M. Shima, K. Rajan and H. Matsui, *Adv. Mater.*, 2004, **16**, 709-712.

96. L. Yu, I. A. Banerjee and H. Matsui, *J. Am. Chem. Soc.*, 2003, **125**, 14837-14840.

97. M. Endo, H. X. Wang, M. Fujitsuka and T. Majima, *Chem. Eur. J.*, 2006, **12**, 3735-3740.

98. H. M. Yi, S. Nisar, S. Y. Lee, M. A. Powers, W. E. Bentley, G. F. Payne, G. R., G. W. Rubloff, M. T. Harris and J. N. Culver, *Nano Lett.*, 2005, **5**, 1931-1936.

99. R. Langer and D. A. Tirell, *Nature*, 2004, **428**, 487.

100. A. V. Persikov and B. Brodsky, *Proc. Natl. Acad. Sci. USA*, 2002, **99**, 1101-1103.

101. M. J. Buehler, *Proc. Natl. Acad. Sci. USA*, 2006, **103**, 12285-12290.

102. S. Frank, R. A. Kammerer, D. Mechling, T. Schulthess, R. Landwehr, J. Bann, Y. Guo, A. Lustig, H. P. Bachinger and J. Engel, *J. Mol. Biol.*, 2001, **308**, 1081-1089.

103. Y. Tao, S. V. Strelkov, V. V. Mesyanzhinov and M. G. Rossmann, *Structure*, 1997, **5**, 789-798.

104. J. Baum and B. Brodsky, *Cur. Opin. Struct. Biol.*, 1999, **9**, 122-128.

105. M. Yin, Y. Gu, I. L. Kuskovsky, T. Andelman, Y. Zhu, G. F. Neumark and S. O'Brien, *J. Am. Chem. Soc.*, 2004, **126**, 6206.

106. J. Stetefeld, S. Frank, M. Jenny, T. Schulthess, R. A. Kammerer, S. Boudko, R. Landwehr, K. Okuyama and J. Engel, *Structure*, 2003, **11**, 339-346.

107. N. Kuznetsova, D. C. Rau, V. A. Parsegian and S. Leikin, *Biophys. J.*, 1997, **72**, 353-362.

108. in *QiaGen Company*, QiaGen Company, 2003, p. 128.

109. J. M. Slocik, R. R. Naik, M. O. Stone and D. W. Wright, *J. Mater. Chem.*, 2005, **15**, 749-753.

110. R. R. Naik, S. J. Stringer, G. Agarwal, S. E. Jones and M. O. Stone, *Nat. Mater.* , 2002, **1**, 169.

111. J. M. Slocik, J. T. Moore and D. W. Wright, *Nano Letter*, 2002, **2**, 169.

112. R. Djalali, Y.-F. Chen and H. Matsui, *J. AM. CHEM. SOC.*, 2002, **124**, 13660.

113. L. Yu, I. A. Banerjee and H. Matsui, *J. AM. CHEM. SOC.*, 2003, **125**, 14837.

114. M. Brust and C. J. Kiely, *Colloids and Surfaces A: Physicochemical and Engineering Aspects*, 2002, **202**, 175.

115. J. M. Slocik, R. R. Naik, M. O. Stone and D. W. Wright, *J. Mater.Chem.*, 2005, **15**, 749.

116. M. Niederberger and H. Colfen, *Physical Chemistry Chemical Physics*, 2006, **8**, 3271.

117. G. Pappalardo, G. Impellizzeri, R. P. Bonomo, T. Campagna, G. Grasso and M. G. Saita, *New J. Chem.*, 2002, **26**, 593.

118. K.-W. Chang and J.-J. Wu, *Adv. Mater.*, 2004, **16**, 545-549.

119. Z. X. Deng and C. D. Mao, *Nano Lett.*, 2003, **3**, 1545-1548.

120. J. M. Kinsella and A. Ivanisevic, *Langmuir*, 2007, **23**, 3886-3890.

121. J. Ziegler, R. T. Chang and D. W. Wright, *J. Am. Chem. Soc.*, 1999, **121**, 2395-2400.

122. Q. Wang, T. W. Lin, L. Tang, J. E. Johnson and M. G. Finn, *Angew. Chem. Int. Ed.*, 2002, **41**, 459-462.

123. L. E. Greene, B. D. Yuhas and P. D. Yang, *Inorg. Chem.*, 2006, **45**, 7535-7543.

124. Z. R. Tian, J. A. Voigt, J. Liu, H. Konishi and H. Xu, *Nature Mater.*, 2003, **2**, 821-826.

125. M. Umetsu, M. Mizuta, K. Tsumoto, S. Ohara, S. Takami, H. Watanabe, I. Kumagai and T. Adschiri, *Adv. Mater.*, 2005, **17**, 2571-2575.

126. M. Yin, Y. Gu, I. L. Kuskovsky, T. Andelman, Y. Zhu, G. F. Neumark and S. O'Brien, *J. Am. Chem. Soc.*, 2004, **126**, 6206-6207.

127. B. Liu and H. C. Zeng, *Langmuir*, 2004, **20**, 4196-4204.

128. F. Li, Y. Ding, P. X. X. Gao, X. Q. Xin and Z. L. Wang, *Angew. Chem. Intl. Ed.*, 2004, **43**, 5238-5242.

129. L. E. Greene, M. Law, J. Goldberger, F. Kim, J. C. Johnson, Y. F. Zhang, R. J. Saykally and P. D. Yang, *Angew. Chem. Intl. Ed.*, 2003, **42**, 3031-3034.

130. D. Kisailus, B. Schwenzer, J. Gomm, J. C. Weaver and D. E. Morse, *J. Am. Chem. Soc.*, 2006, **128**, 10276-10280.

131. S. H. Jung, E. Oh, K. H. Lee, Y. Yang, C. G. Park, W. J. Park and S. H. Jeong, *Cryst. Growth Design*, 2008, **8**, 265-269.

132. Q. J. Yu, C. L. Yu, H. B. Yang, W. Y. Fu, L. X. Chang, J. Xu, R. H. Wei, H. D. Li, H. Y. Zhu, M. H. Li, G. T. Zou, G. R. Wang, C. L. Shao and Y. C. Liu, *Inorg. Chem.*, 2007, **46**, 6204-6210.

133. A. P. A. Oliveira, J. F. Hochepied, F. Grillon and M. H. Berger, *Chem. Mater.*, 2003, **15**, 3202-3207.

134. S. Brown, M. Sarikaya and E. Johnson, *J. Mol. Biol.*, 2000, **299**, 725-735.

135. R. R. Naik, S. J. Stringer, G. Agarwal, S. E. Jones and M. O. Stone, *Nature Mater.*, 2002, **1**, 169-172.

136. J. N. Cha, K. Shimizu, Y. Zhou, S. C. Christiansen, B. F. Chmelka, G. D. Stucky and D. E. Morse, *Proc. Natl. Acad. Sci. USA*, 1999, **96**, 361-365.

137. D. Hennings, M. Klee and R. Waser, *AdV. Mater.*, 1991, **3**, 334.

138. R. E. Newnham, *MRS Bull.*, 1997, **22**, 20.

139. O. Rusina, A. Eremenko, G. Frank, H. P. Strunk and H. Kisch, *Angew.Chem., Int. Ed.*, 2001, **40**, 3993.

140. J. J. Urban, W. S. Yun, Q. Gu and H. Park, *J. Am. Chem. Soc.*, 2002, **124**, 1186.

141. D. Yu, J. Wu, L. Zhou, D. Xie and S. Wu, *Compos. Sci. Technol.* , 2000, **60**, 499.

142. T. Imai, Y. Nishida, M. Yamada, I. Shirayanagi and H. Matsubara, *J. Mater.Sci. Lett.*, 1987, **6**, 1257.

143. H. Y. Zhu, Y. Lan, X. P. Gao, S. P. Ringer, Z. F. Zheng, D. Y. Song and J. C. Zhao, *J. Am. Chem. Soc.*, 2005, **127**, 6730.

144. A. Fujishima, K. Hashimoto and T. Watanabe, *TiO2 Photocatalysis Fundamentals and Applications*, BKC, Inc., Tokyo, 1999.

145. M. S. Chen and D. W. Goodman, *Science*, 2004, **306**, 252.

146. J. D. Stiehl, T. S. Kim, S. M. McClure and C. B. Mullins, *J. Am. Chem.Soc.*, 2004, **126**, 13574.

147. S. U. M. Khan, M. A. Shahry and W. B. Ingler, Jr. , *Science*, 2002, **297**, 2243.

148. M. Wagemaker, A. P. M. Kentgens and F. M. Mulder, *Nature*, 2002, **418**, 397.

149. L. Kavan, M. Kalbac, M. Zukalova´, I. Exnar, V. Lorenzen, R. Nesper and M. Graetzel, *Chem. Mater.*, 2004, **16**.

150. X. P. Gao, H. Y. Zhu, G. L. Pan, S. H. Ye, Y. Lan, F. Wu and D. Y. Song, *J. Phys. Chem. B*, 2004, **108**, 2868.

151. M. Gratzel, *Nature*, 2001, **414**, 338.

152. Y. I. Kim, S. Salim, M. Huq and T. E. Mallouk, *J. Am. Chem. Soc.* , 1991, **113**, 9561.

153. T. Sasaki, M. Watanabe, H. Hashizume, H. Yamada and H. Nakazawa, *J. Am. Chem. Soc.* , 1996, **118**, 8329.

154. N. Sukpirom and M. M. Lerner, *Chem. Mater.* , 2001, **13**, 2179.

155. T. Kasuga, M. Hiramatsu, A. Hoson, T. Sekino and K. Niihara, *Langmuir*, 1998, **14**, 3160.

156. A. L. Linsebigler, G. Lu and J. T. Yates, *Chem. Rev.* , 1995, **95**, 735.

157. L. Yu, I. A. Banerjee and H. Matsui, *J. Mater. Chem.*, 2004, **14**, 739.

158. Q. Chen, W. Zhou, G. Du and L. M. Peng, *Adv. Mater.*, 2002, **14**, 1208.

159. X. Sun and Y. Li, *Chem.-Eur. J.* , 2003, **9**, 2229.

160. J. H. Jung, H. Kobayashi, K. J. C. van Bommel, S. Shinkai and T. Shimizu, *Chem. Mater.* , 2002, **14**, 1445.

161. Z. Y. Yuan, W. Zhou and B. L. Su, *Chem. Commun.* , 2002, 1202.

162. H. Y. Zhu, X. P. Gao, Y. Lan, D. Y. Song, Y. X. Xi and J. C. Zhao, *J. Am.Chem. Soc.* , 2004, **126**, 8380.

163. M. Zhang, Z. S. Jin, J. W. Zhang, X. Y. Guo, J. J. Yang, W. Li, X. D. Wang and Z. J. Zhang, *J. Mol. Catal. A: Chem.*, 2004, **217**, 203.

164. H. B. Yin, Y. Wada, T. Kitamura, S. Kambe, S. Murasawa, H. Mori, T. Sakata and S. Yanagida, *J. Mater. Chem.*, 2001, **11**, 1694.

165. T. Sugiura, T. Yoshida and H. Minoura, *Electrochem. Solid-State Lett.* , 1998, **1**, 175.

166. H. Tokudome and M. Miyauchi, *Chem. Commun.*, 2004, 958.

167. R. Z. Ma, T. Sasaki and Y. Bando, *J. Am. Chem. Soc.*, 2004, **126**, 10382.

168. J. G. Huang, T. Kunitake and S. Y. Onoue, *Chem. Commun.*, 2004, 1008.

169. M. L. Steigerwald and L. E. Brus, *Acc. Chem. Res.*, 1990, **23**, 183.

170. T. Sasaki, S. Nakano, S. Yamauchi and M. Watanabe, *Chem. Mater.*, 1997, **9**, 602.

171. K. Nagaveni, G. Sivalingam, M. S. Hegde and G. Madras, *Appl. Catal. B.* , 2004, **48**, 83.

172. O. d'Hennezel and D. E. H. Ollis, *Chim. Acta* 2001, **84**, 3511.

173. A. I. Hochbaum and P. Yang, *Chem. Rev.*, 2009, **109**, XXX.

174. X. Chen and S. S. Mao, *Chem. Rev.*, 2007, **107**, 2891.

175. Y. Bessekhouad, D. Robert and J. V. J. Weber, *Photochem. Photobiol.,A*, 2003, **157**, 47.

176. G. Oskam, A. Nellore, R. L. Penn and P. C. Searson, *J. Phys. Chem.B*, 2003, **107**, 1734.

177. T. Sugimoto, *AdV. Colloid Interface Sci.*, 1987, **28**, 65.

178. H. Zhang and J. F. Banfield, *Chem. Mater.*, 2005, **17**, 3421.

179. C.-C. Wang and J. Y. Ying, *Chem. Mater.*, 1999, **11**, 3113.

180. D. Li and Y. Xia, *Nano Lett.*, 2003, **3**, 555.

181. Y. Lei, L. D. Zhang and J. C. Fang, *Chem. Phys. Lett.*, 2001, **338**, 231.

182. W.-S. Chae, S.-W. Lee and Y.-R. Kim, *Chem. Mater.*, 2005, **17**, 3072.

183. K.-I. Sano, H. Sasaki and K. Shiba, *Langmuir*, 2005, **21**, 3090.

184. I. A. Banerjee, G. Muniz, S.-Y. Lee and H. Matsui, *Journal of Nanoscience and Nanotechnology*, 2007, **7**, 1.

185. K.-I. Sano and K. Shiba, *J. Am. Chem. Soc.*, 2003, **125**, 14234.

186. A. Berkessel and D. A. HeÂrault, *Angew. Chem. Int. Ed.*, 1999, **38**, 102.

187. F. C. Meldrum and H. Colfen, *Chem. Rev.*, 2008, **108**, 4332.

188. H. Colfen and S. Mann, *Angew. Chem. Int. Ed.*, 2003, **42**, 2350.

189. D. Kisailus, J. H. Choi, J. C. Weaver, W. J. Yang and D. E. Morse, *Adv. Mater.*, 2005, **17**, 314.

190. L. L. Brott, R. R. Naik, D. J. Pikas, S. M. Kirkpatrick, D. W. Tomlin, P. W. Whitlock, S. J. Clarson and M. O. Stone, *Nature*, 2001, **413**, 291.

191. J. M. Whitling, G. Spreitzer and D. W. Wright, *Adv. Mater.* , 2000, **12**, 1377.

192. S. Y. Lee, E. Royston, J. N. Culver and M. T. Harris, *Nanotechnology*, 2005, **16**, S435.

193. T. Douglas and M. Young, *Adv. Mater.* , 1999, **11**, 679.

194. A. Chatterji, W. F. Ochoa, T. Ueno, T. W. Lin and J. E. Johnson, *Nano Lett.*, 2005, **5**, 597.

195. D. Walsh, L. Arcelli, T. Ikoma, J. Tanaka and S. Mann, *Nature Mater.*, 2003, **2**, 386.

196. K. I. Sano, H. Sasaki and K. Shiba, *Langmuir*, 2005, **21**, 3090.

197. S. W. Lee, C. B. Mao, C. E. Flynn and A. M. Belcher, *Science*, 2002, **296**, 892.

198. Z. X. Deng and C. D. Mao, *Nano Lett.*, 2003, **3**, 1545.

199. X. Gao and H. Matsui, *Adv. Mater.*, 2005, **17**, 2037.

200. S. H. Park, R. Barish, H. Y. Li, J. H. Reif, G. Finkelstein, H. Yan and T. H. LaBean, *Nano Lett.*, 2005, **5**, 693.

201. M. Sarikaya, C. Tamerler, A. K. Y. Jen and K. Schulten, *Nature Mater.*, 2003, **2**, 577.

202. R. R. Naik, S. J. Stringer, G. Agarwal, S. E. Jones and M. O. Stone, *Nature Mater.*, 2002, **1**, 169.

203. I. A. Banerjee, L. Yu and H. Matsui, *Proc. Natl. Acad. Sci. USA*, 2003, **100**, 14678.

204. J. L. Sumerel, W. J. Yang, D. Kisailus, J. C. Weaver, J. H. Choi and D. E. Morse, *Chem. Mater.*, 2003, **15**, 4804.

205. A. V. Persikov and B. Brodsky, *Proc. Natl. Acad. Sci., U.S.A.*, 2002, **99**, 1101

206. J. Stetefeld, S. Frank, M. Jenny, T. Schulthess, R. A. Kammerer, S. Boudko, R. Landwehr, K. Okuyama and J. Engel, *Structure*, 2003, **11**, 339.

207. S. Frank, R. A. Kammerer, D. Mechling, T. Schulthess, R. Landwehr, J. Bann, Y. Guo, A. Lustig, H. P. Bachinger and J. Engel, *J. Mol. Biol.*, 2001, **308**, 1081.

208. F. W. Studier, *Protein Expression Purification*, 2005, **41**, 207.

209. N. Kuznetsova, D. C. Rau, V. A. Parsegian and S. Leikin, *Biophys. J.*, 1997, **72**, 353.

210. E. W. Meijer and M. H. P. van Genderen, *Nature* 2003, **426**, 128.

211. M. P. Pileni, *Nat. Mater.*, 2003, **2**, 145.

212. F. Jones, H. Colfen and M. Antonietti, *Colloid Polym. Sci.*, 2000, **278**, 491.

213. T. Luchian, S. H. Shin and H. Bayley, *Angew. Chem., Int. Ed.*, 2003, **42**, 3766.

214. M. L. Flenniken, D. A. Willits, S. Brumfield, M. J. Young and T. Douglas, *Nano Lett.*, 2003, **3**, 1573.

215. R. A. Mcmillan, C. D. Paavola, J. Howard, S. L. Chan, F. J. Zaluzec and J. D. Trent, *Nat. Mater.*, 2002, **1**, 247.

216. Q. Wang, T. Lin, L. Tang, J. E. Johnson and M. G. Finn, *Angew. Chem.,Int. Ed.* , 2002, **41**, 459.

217. Y.-W. Jun, J.-S. Choi and J. Cheon, *Angew. Chem., Int. Ed.*, 2006, **45**, 3414.

218. Y. N. Xia, P. D. Yang, Y. G. Sun, Y. Y. Wu, B. Mayers, B. Gates, Y. D. Yin, F. Kim and Y. Q. Yan, *Adv. Mater.*, 2003, **15**, 353.

219. V. F. Puntes, K. M. Krishnan and A. P. Alivisatos, *Science*, 2001, **291**, 2115.

220. R. Djalali, J. Samson and H. Matsui, *J. AM. CHEM. SOC.*, 2004, **126**, 7935.

221. N. Nuraje, K. Su, A. Haboosheh, J. Samson, E. P. Manning, N.-l. Yang and H. Matsui, *Adv. Mater.*, 2006, **18**, 807.

222. M. Maillard, S. Giorgio and M. P. Pileni, *AdV. Mater.* , 2002, **14**, 1084.

223. T. C. Wang, M. F. Rubner and R. E. Cohen, *Langmuir* 2002, **18**, 3370.

224. M. Fang, P. S. Grant, M. J. McShane, G. B. Sukhorukov, V. O. Golub and Y. M. Lvov, *Langmuir* 2002, **18**, 6338.

225. D. J. Pochan, J. P. Schneider, J. Kretsinger, B. Ozbas, K. Rajagopal and L. Haines, *J. Am. Chem. Soc.*, 2003, **125**, 11802.

226. D. T. Bong, T. D. Clark, J. R. Granja and M. R. Ghadiri, *Angew. Chem.Int. Ed.*, 2001, **40**, 988.

227. J. D. Hartgerink, E. Beniash and S. I. Stupp, *Science*, 2001, **294**, 1684.

228. G. Agarwal, R. R. Naik and M. O. Stone, *J. Am. Chem. Soc.*, 2003, **125**, 7408.

229. M. Sarikaya, C. Tamerler, A. K. Y. Jen and K. Schulten, *Nat. Mater.*, 2003, **2**, 577.

230. K. M. Roth, Y. Zhou, W. Yang and D. E. Morse, *J. AM. CHEM. SOC.*, 2005, **127**, 325.

231. K. SHIMIZU, J. CHA, G. D. STUCKY and D. E. MORSE, *Proc. Natl. Acad. Sci.*, 1998, **95**, 6234.

232. J. N. CHA, K. SHIMIZU, Y. ZHOU, S. C. CHRISTIANSEN, B. F. CHMELKA, G. D. STUCKY and D. E. MORSE, *Proc. Natl. Acad. Sci.*, 1999, **96**, 361.

233. D. E. Morse, *Trends Biotechnol.* , 1999, **17**, 230.

234. J. N. Cha, K. Shimizu, Y. Zhou, S. C. Christiansen, B. F. Chmelka, T. J. Deming, G. D. Stucky and D. E. Morse, *Mater. Res. Soc. Symp. Proc.*, 2000, **599**, 239.

235. G. Dodson and A. Wlodawer, *Trends Biochem. Sci.*, 1998, **23**, 347.

236. M. Kogiso, S. Ohnishi, K. Yase, M. Masuda and T. Shimizu, *Langmuir*, 1998, **14**, 4978.

237. H. Matsui, S. Pan, B. Gologan and S. H. Jonas, *J. Phys. Chem. B*, 2000, **104**, 9576.

238. T. Shimizu, M. Masuda and H. Minamikawa, *Chem. Rev.*, 2005, **105**, 1401.

239. Q. Ji, S. Kamiya, J.-H. Jung and T. Shimizu, *J. Mater. Chem.*, 2005, **15**, 743.

240. H. Matsui and B. Gologan, *J. Phys. Chem. B*, 2000, **104**, 3383.